ROCOST

Robust and cost-efficient hard part turning of transmission components

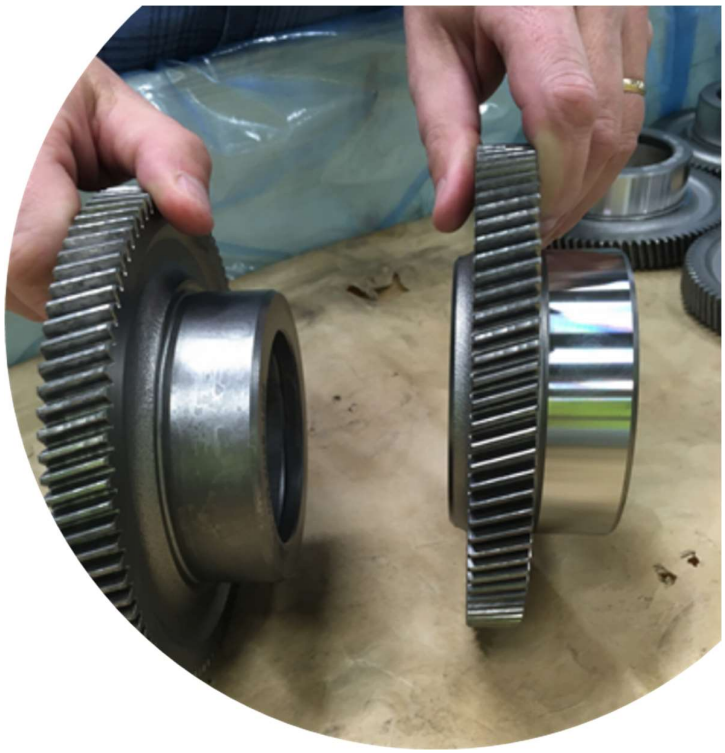

Författare: Ulrika Brohede[1], Hans Kristofferssen[2], Yaoxuan Zhu[3], Anna Ganea[4], Thomas Björk[5], Harald Nyberg[6], Alexander Drott[7], Kim Wallin[7], Magnus Svensson[8], Emil Stålnacke[1], Albin Stormvinter[2], Pär Andersson[2].

[1]Swerim AB, [2]RISE, [3]KTH IIP, [4]Sandvik Coromant, [5]OVAKO, [6]Scania CV, [7]Volvo LV, [8]Swepart Transmission.

Datum: 2021-04-15
Projekt inom Hållbar produktion

FFI Fordonsstrategisk Forskning och Innovation
VINNOVA Energimyndigheten TRAFIKVERKET
FKG VOLVO SCANIA VOLVO

Contents

1 Sammanfattning på svenska

Detta är slutrapporten för ett projekt i samarbete mellan parter längs produktionskedjan, från ståltillverkare till komponenttillverkare av transmissionskomponenter.
Samband mellan stålsort och sätthärdning och samband mellan verktygsförslitning och processdynamik i bearbetningsprocessen undersöktes och relaterades till mikrostrukturen i materialet. Syftet var att ge insikt i hur sätthärdingsprocessen kan optimeras för att ge en robust och kostnadseffektiv hårdsvarvningsprocess för transmissionskomponenter, med målet att nå 50% ökad produktivitet. Med produktivitet menas i detta fall summan av processer som påverkar en kontrollerad och förutsägbar skärförslitning – robusthet.
Labkomponenter tillverkades av två stålsorter: Ovako 236F (20MnCr5) and Ovako 159S (18CrNiMo7-6). De sätthärdades med målet att få 0.64, 0.72 och 0.80 vikts% ytkolhalt och anlöptes vid 160 °C and 180 °C temperatur för att uppnå olika hårdhet. Hårdsvarvning genomfördes i test liknade både grov- och finbearbetning vid 150-275 m/min. Skärförslitningen analyserades numeriskt (grop- och fasförslitning). Restaustenithalten mättes även på bearbetade komponenter. En metod för att utvärdera robustheten i processen utvecklades från insamlad data av vibration, ljud och maskinström.

Materialegenskaperna (Vickers hårdhet, HV och restaustenit, RA) uppmättes i labkomponenterna till: 750-800 HV1 och 15-25% RA i 236F, och 700-750 HV1 och 20-35% RA i S159. Fasförslitningen (VB) spred från 10 till 80 µm för båda stålsorter och gropförslitningen (KT) spred mellan 3 till 25 µm i för 236F och 8 till 50 µm i 159S.

Några generella trender kunde definieras från hårdsvarvningstesten av labkomponenter:

- Grovbearbetningen påverkades av det yttersta skalet och distorsion i form av mer förslitning och ökad spridning.
- I 159S-stålet är det möjligt att kontrollera skärförslitningen:
    - Inom ett begränsat område ger ökad RA och HV ökad skärförslitning.
    - Ökad restaustenit (alt. kolhalt) ökar risken för skärbrott.
- 236F-stålet är inte lika känsligt för variationer.
    - Liten effekt från RA och HV på skärförslitning.
- Olika stålsorter med samma utfall från härdningen gällande RA och HV ger olika skärförslitning.
    - Vid högre skärhastighet genererar 236F mindre skärförslitning än 159S, vid samma RA och HV

Vid bearbetning ökade RA i det yttersta skiktet, för att snabbt sjunka utifrån RA-profil uppmätt efter sätthärdingen. En ökad fasomvandlingseffekt i RA-området som visade ökad skärförslitning kunde identifieras.

För att verifiera analysmetoden som togs fram för robusthet, behövs mer data. För att prediktera verktygsförslitning krävs längre tid av datainsamling under bearbetningen för att följa förslitningsprocessen.

Mappning av tre valda demonstratorer från tre olika produktionsenheter visade:

- Skillnader i utfall från härdningen med avseende på mätta materialegenskaper för olika batcher / produktionsrutter.
- Viss skillnad i bearbetbarhet men inga tydliga korrelationer till materialdata.
- Större påverkan från andra faktorer, tex distorsion/dimension.

Slutsatsen är att produktiviteten kan förbättras genom en kontrollerad produktion längs hela värdekedjan!

2 Executive summary

This is the final report for a collaboration project between partners along the production chain, from steel manufacturing to transmission component manufacturing. Relations between steel grade and carburizing, and relations between tool wear and process dynamics were investigated and related to the material microstructures. The goal was to provide know-how on how to optimize the carburized case of typical transmission components to provide a robust and cost-efficient hard turning process, aiming for a 50% productivity increase. Productivity is here defined as the sum of processes influencing a controlled and predictable tool wear – robustness.
Lab-components were produced from two steel grades: Ovako 236F (20MnCr5) and Ovako 159S (18CrNiMo7-6). They were case hardened targeting 0.64, 0.72 and 0.80 mass% C and tempered at 160 °C and 180 °C to differentiate hardness. Hard turning was performed in both a roughing-like and a finishing-like process at 150-275 m/min. Tool wear was numerically measured (crater depth and flank wear). Retained austenite was also measured after machining. A methodology to evaluate the robustness was developed from vibration, sound, and machine current data.

The material properties (Vickers hardness, HV and retained austenite, RA) in the case hardened portion of lab-components ranged from about 750-800 HV1 and 15-25% RA in 236F, and 700-750 HV1 and 20-35% RA in S159. Flank wear (VB) ranged from about 10 to 80 µm in both steels and crater wear (KT) ranged from 3 to 25 µm KT in 236F and from 8 to 50 µm KT 159S.

Some general trends were defined from the hard part turning tests on lab components:

- The roughing setups show influence of outer scale and distortion in terms of more wear and increased spread.
- In steel grade159S there is a possibility to control wear by heat treatment
    - Increased RA and HV drive wear – in selected region
    - Increased RA (%C?) drives risk of edge failure
- Steel grade 236F is less sensitive to variations.
    - Less impact from HV and RA
- Tool wear differs between steels grades at similar hardening outcome.
    - At higher speed, 236F generates less wear than 159S at similar HV, RA

RA increased during machining in the outer-most portion of the case, to rapidly decrease below the measured RA-profile from case hardening. The effect of phase shift was larger in the same RA-window as identified for increased tool wear.

To verify the methodology for robustness analysis more data is needed. For tool wear prediction, longer sampling of machining data following the wear development is needed.

A mapping of three demonstrators at three production sites showed:

- Variations in hardening outcome between batches and supply routes
- Some impact on machinability, but no clear correlation to material properties.
- Variation from other factors dominate (e.g. distortion/dimensions)

In summary the productivity in industrial applications will benefit from controlled production along the whole production chain!

3 Background

Transmissions and gear boxes of vehicles are made of a large number of gears and shafts, bearings, pins, etc. The vast majority are made of carburized, micro-alloyed, wrought and forged steel for carburizing. The parts have an inherent carbon content from the steel mill of some 0.15 to 0.25%C. The 0.5-1 mm outer rim of the machined part is carburized to 0.6-0.8% C and subsequently quenched. Hence, this gives a hard carburized case and a relatively ductile core of the part. The resistance to bending fatigue loads in the gear root, as well as the resistance to superficial damages from contact fatigue in the reciprocating gear flank contacts become excellent. Yet, in case a gear fracture occurs, the core toughness minimizes the risk of complete breakdown of the part.

The parts made with this design include cylindrical gears, conical gears, shafts, planet gears, ring gears, among others. The typical manufacturing route starts from steel bars, through forging and subsequent annealing.
The soft machining may include turning, gear cutting, broaching, shaping, de-burring, etc. After carburizing hardening, all parts are hard machined. Gear flanks are ground, honed or lapped. Shafts, gear faces and bearing seats for bearings are frequently hard turned. Though, both processes are used simultaneously. CNC machines that enable both hard turning and grinding are becoming more and more frequent.

The breakthrough of hard part turning some 20 years ago is primarily attributed to the development of polycrystalline cubic boron nitride (PCBN) as tool material. PCBN increases the production efficiency, and it responds to demands of surface quality of the part. Cycle times can be shortened, and subsequent grinding becomes obsolete, as compared to the manufacturing routes previously used, consequently, hard turning is today considered a cost efficient and flexible process. However, the challenge with hard turning have been experiences of unreliability. Scatter in tool life and part's surface quality have been reported. Better control of machine stability, chatter and clamping have been important contributions to minimize such experiences. However, some variations of production efficiency still remain. The steel making plays a decisive role in some cases. It was found in previous research that Ca-treatment aiming at improved machinability, foremost Ovako M-steel, significantly reduces the crater wear of PCBN tools. The tool life of PCBN tooling could be doubled in a case study at Scania in year 2016. Moreover, the cutting speed could be increased from 175 m/min to 225 m/min with retained production efficiency.
A part of that is believed to follow batch to batch variations in the workpiece deliveries from the previous carburizing. Carburized parts have a few characteristics that may contribute to variations in process robustness in PCBN hard turning:

- Distortion, which may lead to intermittent machining in the first cut.
- The inherent gradient of the material characteristics experienced by the cutting edge, including the HTTP, as well as gradients of retained austenite, hardness, and carbon content.
- The big impact of furnace performance and quenching process on the resulting carburizing characteristics.
- Among others

Given the batch-to-batch variations experienced in some recent industrial cases it was believed that there is a big potential to investigate the carburizing process and the resulting carburized layer of the work piece and their link to tool wear and process performance in hard part turning. Hard part turning of carburized steel have been investigated in a large number of publications, PhD thesis, in internal development projects within suppliers of cutting tools, among others. A lot of attention of recent research have been given surface integrity of the hard machined part. However, to the project group's best knowledge, no work has been published in the interface of the carburizing process, the characteristics of the carburized case and PCBN tool wear.

4 Purpose, research questions and target

The project goal of the ROKOST project was, following its title "Robust and cost-efficient hard part turning of transmission components", to increase both the process efficiency and the robustness at the same time. The goal was to provide know-how of how to optimize the carburized case of typical transmission component to provide a robust and cost-efficient hard turning process. The project goal is schematized in Figure 1. In this example, the optimal cutting speed is about 170 m/min. The tool life is in this case 64 min with a scatter of $-5<\sigma<+7$ minutes. A desire to increase the cutting speed, thereby reducing the cycle time, with the current tooling, machine, workpiece, and carburizing, would lead to a tool life of 50 min at 225 m/min. Though, the tool life scatter of $-20<\sigma<+7$ would

become unacceptable for the production efficiency. Instead, the project goal was to enable longer tool life at higher speed with retained scatter, as compared to today's optimum.

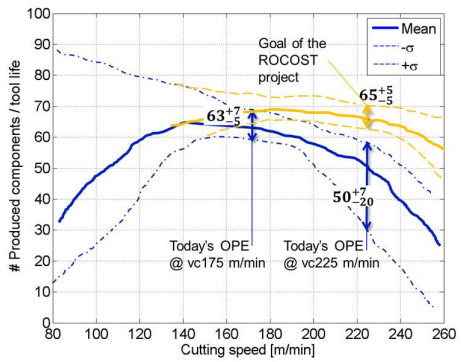

Figure 1. Schematic of today's realistic cutting speed and associated scatter, as well as the goal of the ROKOST project.

4.1 Steel grade

Two steels from Ovako Hofors steel mill were used as work piece materials of the project. The steels are cast to a 420x420 mm^2 square ingot and hot rolled to the desired dimension. Both steels are made with the same metallurgy process, which is basically tuned to minimize the content of large oxide inclusions (D-slags) and thus to meet demands from bearing applications.

Ovako 236 (20MnCr5) is a case-hardening steel with low carbon content but good hardenability reaching good wear resistance due to high surface hardness after hardening. The small grain size benefits in good ductility and fatigue strength. Suitable for gearboxes and axle gears. Ovako 236F is a standard variant with controlled sulphur content for consistent machining properties.
Ovako 159 (18CrNiMo7-6) is a case hardening steel with high toughness. There are several variants which all possess tighter composition ranges compared to the EN-standard. Grade 159S is a variant with increased sulphur content.
The chemical composition for each melt is shown in Table 1Table 1: Chemical composition (wt %) for Ovako 236F and Ovako 159S

Table 1: Chemical composition (wt %) for Ovako 236F and Ovako 159S

	C	Si	Mn	P	S	Cr	Ni	Mo	Cu	V	Al
236F	0,2	0,24	1,15	0,014	0,021	1,17	0,12	0,03	0,236	0,006	0,029
159S	0,16	0,32	0,58	0,005	0,017	1,63	1,43	0,28	0,181	0,009	0,03

The higher alloying content in the Ovako 159 grade will have an effect of increased level of retained austenite content in the carburised layer after quenching. Calculation of martensite start temperature, Ms, and retained austenite, RA, for actual compositions and surface carbon 0,72 wt% using the software JMatPro® gives an indication for this, see Table 2

Table 2: JMatPro calculations of Ms and RA-content for surface carbon content 0,72 wt%

	Ms, °C	$M_{50\%}$, °C	$M_{90\%}$, °C	$RA_{20\,°C}$, %	$RA_{100\,°C}$, %
236F	185	145	51	6	23
159S	176	135	41	8	27

It is clear that JMatPro underestimates the retained austenite level at room temperature. That is why the values for RA-levels at 100 °C also are shown. At this temperature the quenching are stopped or slowed down which can have stabilisation effect on austenite. Another reason for the underestimation could be that the thermodynamic approach used in JMatPro do not take into account the stresses that occurs during quenching and phase transformations and that these stresses can counteract the martensite transformation at later stages.

Carbon influence on steel

In case hardening, carburized austenite transforms into martensite upon rapid quenching. The resulting microhardness – although neglecting effect by grain size and grain boundaries – can be estimated as the sum of two resulting structures: martensite and retained austenite, RA, and is usually measured using microhardness indentation.

$$HV_{estimated} = HV_{RA} * f_{RA} + HV_{mart} * (1 - f_{RA})$$

Martensite hardness, HV_{Mart}, depends on composition – especially carbon content; Low-carbon martensite is softer compared to high-carbon but is much harder than retained austenite, HV_{RA} [Troell et al.[1]]. The carbon content of martensite is inherited from the austenite prior to quenching since the transformation is diffusionless. In addition, carbon content controls the fractions of each structure: higher %C increase retained austenite, f_{RA}, due to decreased start-temperature for martensite formation, i.e., M_s. Furthermore, retained austenite can also transform into martensite during loading (mechanically induced martensite transformation, MIMT), making HV_{RA} challenging to quantify [Hossain et al.[2]]. Ultimately, the extent of MIMT is controlled by the stability of RA [Hossain et al. [3]] (composition dependent, e.g. fraction Cr etc.) and the applied load [Hossain et al. [2]]. Literature is not conclusive on how much MIMT affects hard turning and the subsequent tool wear.
The various effects carbon has on the steel is summarized inTable 3.

Table 3: The influence of carbon content on casehardening steels, related to final hardness.

Steel grade carbon content, %C	Low ◄——► High	
Martensite hardness, HV_{RA}	Low	High
Retained austenite fraction, f_{RA}	Low	High
MIMT-effect	Weak	Strong

Because carbon both increase f_{RA} (soft) and HV_{Mart} (hard), differently carburized steels can display the same $HV_{estimated}$ but have different microstructures and thus different material properties. As exemplified in Figure 2, overall $HV_{estimated}$ can decrease but not reflect increase of HV_{Mart}.

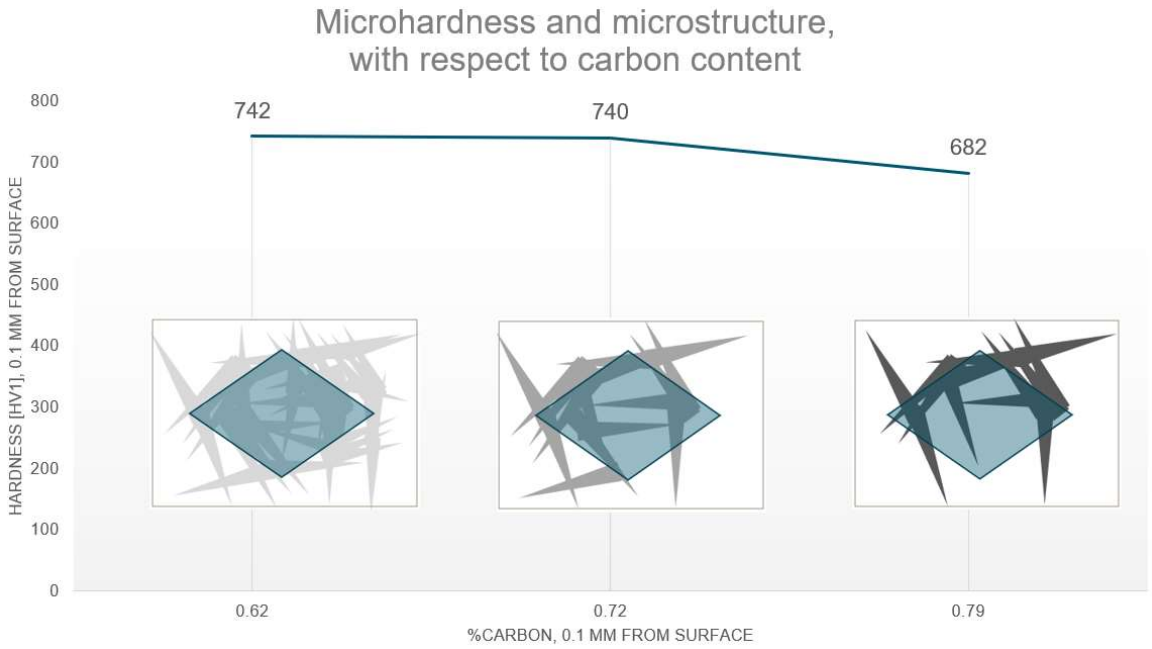

Figure 2: Hardness of 18CrNiMo7-6, carburized at various carbon contents. The illustrations below the hardness value indicate microstructure captured by the indentation zone (blue area) for each carbon content. The grey areas indicate martensite, and white areas retained austenite. High-carbon martensite is represented by darker hue of grey.

4.2 Heat treatment

The present work was inspired by Design of Experiment when planning heat treatments of lab-components. For case-carburized components, carbon content is a key factor that influence most material properties and thus component performance. For this reason, experiments targeted a wide range of realistic surface carbon-contents, that is 0.64, 0.72 and 0.80 mass% C. As previously discussed, two steel grades were used for the experiments. These are representative for the common alloying-concepts MnCr and CrNiMo, when regarding case-carburizing steels. The heat treatments were designed to produce a "flat" carbon profile in the near surface layer, which in turn should generate a deep case with an even retained-austenite content. Hence, a fairer assessment of machinability is possible by reducing the gradient in microstructure, which is often entailed by case-carburize hardening. Apart from researching the effect of carbon content, the effect of tempering was investigated by applying either lower (160°C) or higher (180°C) temperature. Accounting for all these factors an experimental design was set, which is seen from Figure 3

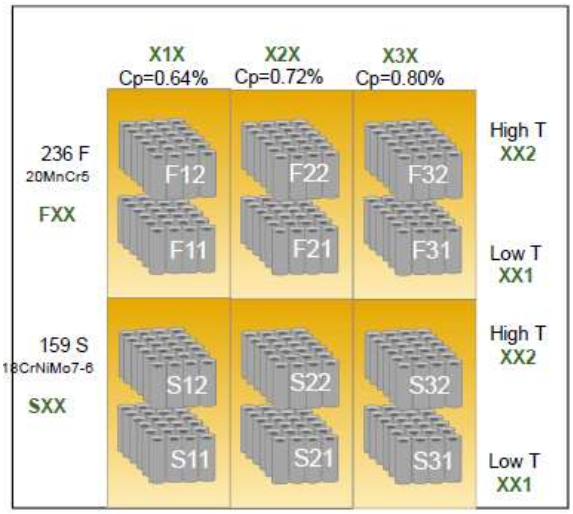

Figure 3: Schematic of experimental design used on lab-components. Including the variant nomenclature used through the report.

4.3 Machining and tool wear studies

Based on industrial experience and earlier investigations [Ånmark et. al.[4] , Ånmark and Björk.[5], Stavlid and Björk[6]] often, a hypothesis is that tool wear will differ depending on the steel characteristics, including residual austenite and hardness (from heat treatment), as well as chemical constituents (from steel selection). These could be expected to influence one or several wear types such as crater wear, flank wear and wear at the secondary edge, as well as tendencies to edge breakages [Boing et. al. [7]].

Laboratory test set-ups, such as [Ånmark et.al.[4], Ånmark and Björk[5], Stavlid and Björk[6]] often exclude the machining of the outer scale, where dimensional irregularities and roughness affects the tool wear. In this study, two approaches were applied; one where the surface zone was included, in order to assess effects in a production-relevant roughing operation, another where the outer layer was removed, to isolate material influences and serve as a more phenomenological study.

The study also includes an investigation of the impact from machining on retained austenite.

In addition to the tool wear studies a robustness study was performed, to investigate how well the material properties and tool wear can be detected and analyzed *in situ* by sensors in machining.

4.4 Robustness

Surface quality of machined component is one of important indicators of quality control in machining process in which the nature of its complexity leads to difficulties in directly building and formulating a precise model to completely elaborate on the correlation between process variables such as machined workpiece, tools, tool condition, CNC machines, cutting parameters and online surface quality and tool wear state in both laboratory and industry environment. Even if a simple model is successfully built with one machining system setup which cannot applied into another. Hence, the development of intelligent machining system has the huge potential on implementing the

robustness or generalization of indirect machine tool and surface quality control, which enables explore and reflect the online complex and nonlinear correlation based on observed online input data during machining process. Intelligent machining system is built on the process control and monitoring system integrating multi-data fusion technology and machine learning algorithms.

In this project, KTH mainly takes responsibility for the initial and exploratory studies on multi-data fusion technique and only few efforts on machine learning algorithm development with the reason that to select the appropriate and reasonable types of or data is prerequisite for later algorithm building and training. The sensor selection totally depends on the evaluation of correlation level between the signal from each potentially selected sensor and relevant surface quality which is surface roughness Ra in this case. The correlation evaluation process is composed of experimental test, signal data collecting and processing, feature extraction and selection and correlation calculation between selected features of each type of sensor and measured surface roughness of machined components.

5 Method

5.1 Work piece preparation

The work pieces for the laboratory tests were made from hot rolled, thick walled tubes of OD=125 mm and ID=65 mm. The test components were machined to the design shown in Figure 4. The outer rim was to be used in hard turning tests. The work piece was to be internally clamped by chuck jaws on the left hand side. The right hand side was prepared for a pipe center clamping.

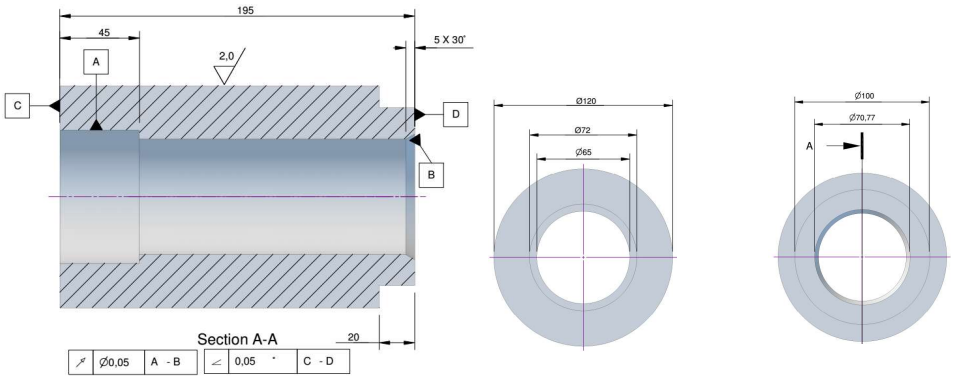

Figure 4. Drawing of the soft machined work piece for laboratory tests.

5.2 Heat treatment

Case-carburizing of lab-components was done using an Ipsen T11 sealed quench furnace with a boost-and-diffusion process. Quenching was done in oil. In total six furnace batches were done, three for each steel grade using the different carbon content set-points. Every furnace load consisted of two baskets with 24 pieces each. After case hardening and washing the two baskets were separated and run with either low- or high tempering temperature. Furnace recipes were designed using AGA-Linde C-calc with set-point at surface depths 0.0 and 0.5 mm for the chosen carbon content. This would produce a recipe that generates a flat carbon profile in the near-surface regime, that is <0.5 mm. This boundary-condition would in-turn generate a quite deep case-depth (CHD) of around 1.5 mm. Simulated carbon contents are compared to experimentally determined in Table 4.

Table 4: Overview of simulated and experimentally determined carbon contents. Measurements were done on smaller test-bars that were cut from the lab-component tubes prior to heat treatment and used in the lathe to collect chips from controlled turning depths. Carbon content was experimentally determined by subsequent LECO analysis of chips.

		Simulated with C-calc			Exp. determined	
		0 mm	**0.5 mm**	**CHD**	**<0.05 mm**	**0.4-0.5 mm**
Series 0.64	**236F (F11/12)**	0.64	0.64	1.51	0.63	0.70
	159S (S11/12)	0.62	0.61	1.42	0.61	0.64
Series 0.72	**236F (F21/22)**	0.72	0.72	1.50	0.71	0.78
	159S (S21/22)	0.69	0.69	1.42	0.73	0.75
Series 0.80	**236F (F31/32)**	0.81	0.78	1.57	0.80	0.85
	159S (S31/32)	0.78	0.75	1.48	0.81	0.83

5.3 Characterization after heat treatment

Carbon content measurements were done on smaller test-bars, that were cut from the lab-component tubes prior to heat treatment and used in the lathe to collect chips from controlled turning depths. Carbon content was experimentally determined by subsequent LECO analysis of chips.

Hardness measurements were done in accordance with SS-EN ISO 6507-1. Measurements were done on ground and polished cross-sections of lab-components using a fully automated micro-hardness tester Qness Q10A+. Hardness profiles were done with HV1 indentations. Hardness results are presented as the mean values of three indentations/profiles.

Retained austenite (RA) measurements were performed by x-ray diffraction technique (XRD) using a Xstress ROBOT/Xtronic 1.12.1-system and destructive layer removal by electro polishing with saturated NaCl solution. For these measurements, the system was equipped with a Cr X-ray tube (λ:0.229 nm). RA measurements were done in accordance with ASTM E975-03 using a 3 mm collimator. The ferrite and austenite peaks were fitted using Pearson VII and Gauss, respectively.

5.4 Tool wear studies

In comparison to industrial applications, the ideal evaluation of tool wear would be performed in the outer layer of the hardened steel material. However, experience from laboratory tool wear evaluations tells that such evaluations are associated with large variability due to dimensional and other variations. While these are important for the full understanding of the industrial application, it was deemed necessary to separate those effects from actual material variations. Therefore, the below lay-out was selected, Figure 5.

Based on hardness and retained austenite profiles originating from the different carburizing processes, the following zones were defined:

Zone 1: The first cut, including dimensional run-out and surface roughness, at 0-0,1 mm from the surface.

Zone 2: Cuts done in virtually constant hardness and retained austenite of the depth profile.

Zone 3: Cuts done at variable hardness and retained austenite, at a depth where the retained austenite and hardness profiles are decreasing.

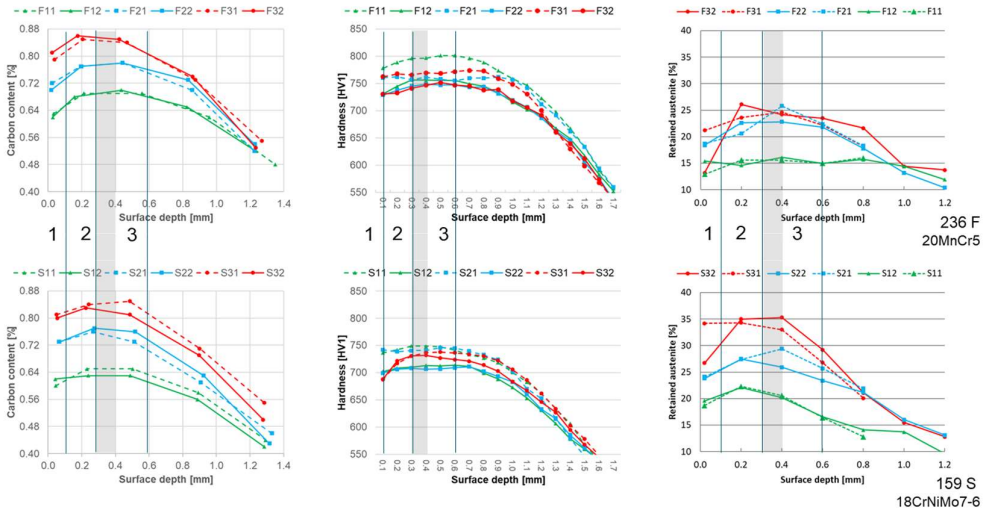

Figure 5: indicate the different cutting zones per depth profile of the material parameters investigated.

The tool wear studies were performed in three different lathes (and reported separately), for investigations of:

- the tool wear from material properties **(5.4.1)**
- the tool wear from an industry like material including surface effects **(5.4.2)**
- the robustness in machining affected by the different variants **(5.5)**

See all set-ups in Table 5.

Table 5: Test set-ups at the three sites, showing cutting lengths, machined zones and number of lab components used/variant.

Test	Lathe	Chip cut length, CCL [m]	Run in zone	Run at depth	No. of lab comp./var.
SWE	OKUMA LB300-M	2634	1+2	3 cuts 0-0,3 mm	2 parts
KTH-SWE	OKUMA LB300-M	2558	1+2	3 cuts 0-0,3 mm	2 parts
KTH-KTH	SWETURN	2558	1+2	3 cuts 0-0,3 mm	2 parts
COR	OKUMA	880	1	1 cut 0-0.1 mm	2 parts
		877	2	1 cut 0.1-0.2 mm	2 parts
		873	3	1 cut 0.2-0.3 mm	2 parts
		1751	Mixed	2 cuts, varied	
COR+	OKUMA	1625	2+3	4 cuts 0.1-0.5 mm	1 part

The chip cut length for one cut on one part is approximately 440 m (varying slightly depending on clamping and adjustment for component diameter for the different cuts). Different cut lengths per edge are achieved by different numbers of cuts per parts, and/or different number of parts used.

Cutting parameters were chosen to be production relevant:
Feed (f) = 0,15 mm
Cutting depth (ap) = 0,1 mm
Speed (Vc) = 150 m/min, 210 m/min*, 270 m/min
**only in COR and COR+ tests.*

Clamping was done with soft, wide clamping jaws, a 60° tip angle stud (tube stud) from Bell Head Centers was used is all test set-ups. The insert used was an uncoated PCBN tool CNGA10408S01525 (CB7114) (with 0,8 mm nose radius. The land width and angle were standard for the article, (width=0,15 mm, angle=25°). The inserts used were an un-coated variant of the commercial grade CB7115. It was selected to run un-coated to simplify wear analysis, all while wear progression is essentially the same as for a coated tool.

The tool wear was analyzed by SEM imaging (JEOL 7000F at Swerim and Zeiss Supra 40 at Sandvik Coromand) and numerical evaluation of flank- and crater wear by infinite focus measurements (Alicona SL at Swerim and Sandvik Coromant).
The numerical evaluation of flank wear, crater depth and wear rate was done by standard procedures according to: [Boing et. al. [7]] and surface topography was analyzed according to the ISO 25178-2:2012 standard.

5.4.1 Phenomenological tool wear, influence from material

The tests COR and COR+ were designed to minimize effects of varying component dimensions. This was done by a separate clean cut to remove the outermost material and thereby achieve consistent dimensions before test.

While this does not mimic such production operations that involve some degree of roughing, it significantly reduces scatter and is perceived as a means to isolate the effect of material variations (residual austenite and hardness) on wear, from those of dimensional variability. This is referred to here as a phenomenological tool wear study, but can also be seen as a test representative of finishing applications. (It can also be noted that the run-out on the test components was larger than in many industrial applications, and probably subject of variations between variants.)

In test layout COR, different cutting tool edges were used to machine different zones; zone 1 (the clean cut), zone 2 and zone 3, see Table 5. The intention was to allow comparison of wear in these zones, with the double purpose of

- Assessing wear dependency on additional combinations of material properties (declining hardness in deeper zones),
- Indicate on the relevancy of running tests in multiple zones. If seen to differ significantly, this should be considered for tests run in several zones.

In test layout COR+, run to longer test time, four cuts were made, thus combining zones 2 and 3, but still without the outer layer - for best consistency and a phenomenological approach.

5.4.2 Production like tool wear, influence form material and system set-up

The tests SWE, KTH/SWE and KTH/KTH were designed to consider both the dimensional run-out and the finishing cut. One edge was used for three cuts in two components, corresponding to ~880 ccl in the surface zone at 0,1 mm depth of cut and two cuts corresponding to ~1755 meters in the zone between 0,1-0,3 mm depth. Table 5.
The intention of the test design was to mimic a production relevant machining operation to investigate the magnitude of influence from the material properties and run-out effects.

5.5 Robustness

As mentioned in previous chapter, the research work from KTH is mainly based on online experiment test and signal data collection and offline signal processing, feature extraction from each signal and prediction accuracy of surface roughness as performances criteria among different algorithms based on different types of signals both in time domain and frequency domain. The surface roughness prediction system follows the procedure illustrated in Figure 6, the cutting parameters such as cutting speed, feed rate, depth of cut are setup to control the hard part machining process in which signals composed of vibration, audible sound and motor current are collected and recorded for post-processing. Then collected signal post-processing is based on the generic procedure of data processing method which is commonly applied into data science or big data area by machine learning engineer and data engineer or scientist before putting into the algorithms as input data for final surface roughness prediction.

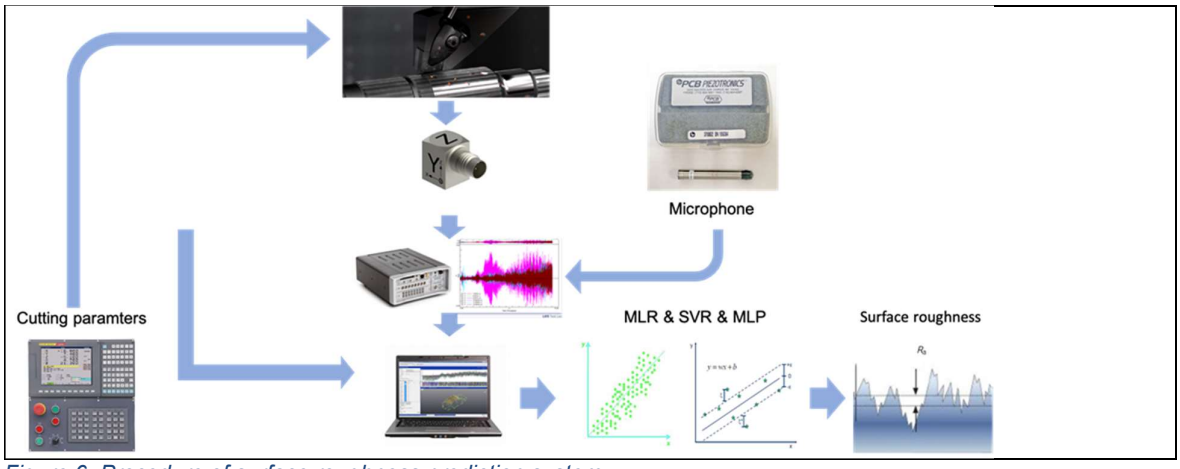

Figure 6: Procedure of surface roughness prediction system

5.5.1 Sensor selection and installation

With the consideration of practical use in local industry and miniaturization of each sensor itself, in this study, accelerometer and microphone are selected to build multi-sensor data system in which mechanical vibration in 3 axes direction (a_p, a_f, a_c) and audible sound are captured by triaxle piezoelectric accelerometer (Dytran 3023A2) with frequency bandwidth 20 Hz -10k Hz and microphone with frequency bandwidth 3.75 Hz -20k Hz and 15.5 dB inherent noise respectively. The accelerometer and audible microphone are separately located on the tip of the tool holder behind the insert (Position1 in Figure 7) and on the top of jaw chunk (Position2 in Figure 7). Signal from two sensors are registered independently in each sampling area (SA1 and SA2) where corresponding surface roughness are measured. Then signals are processed and recorded by Siemens LMS Test Lab system with sampling frequency 2.5 times more than bandwidth frequency of each sensor in order to obtain adequate signal resolution.

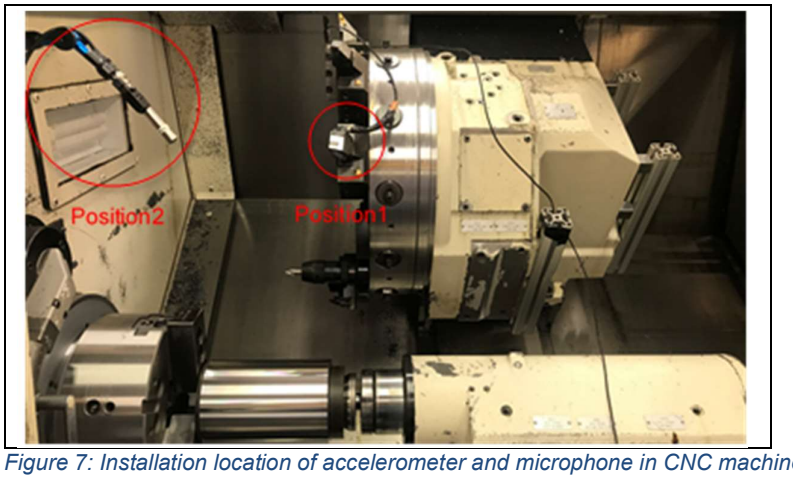

Figure 7: Installation location of accelerometer and microphone in CNC machine

5.5.2 Surface roughness measurement

The parameters selected for the characterization of surface quality are mean deviation of the profile (R_a), 10 points height (R_z) and maximum peak to valley (R_t) measured by Mitutoyo SJ-210 profilometer with 0.8 length of cut-off and 5 sampling points. In each sampling area (SA1 and SA2), the selected parameters are measured as the average values of three equidistant measures in 120 degree rotation: 0 degree, 120 degree and 240 degree (Figure 8). The surface roughness parameters measured in each sampling area are correlated to the signals registered in machining test.(Figure 8)

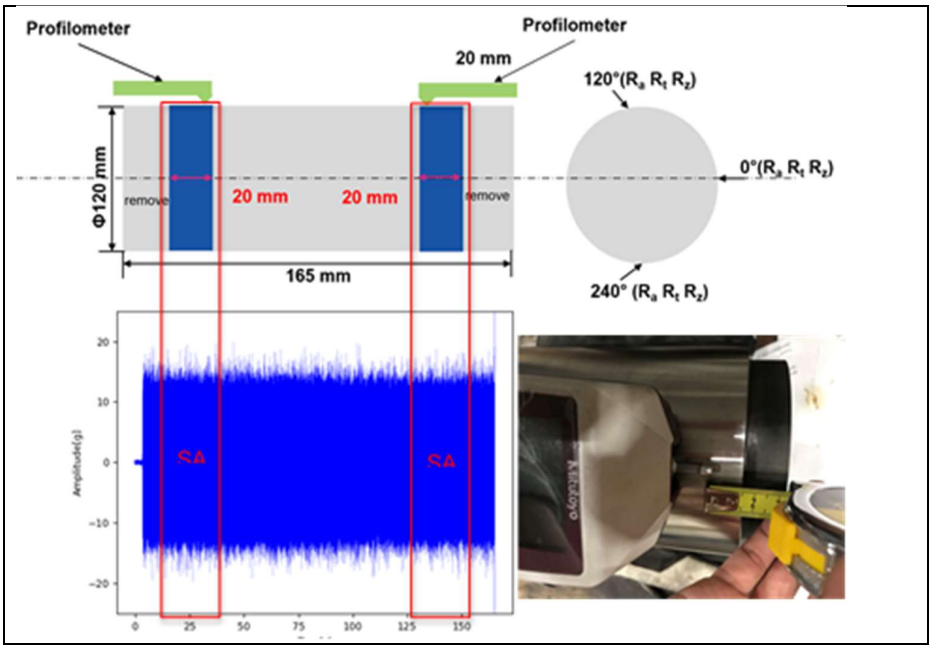

Figure 8 Sampling areas (SA1 and SA2) and corresponding registered signal in time domain

5.5.3 Machining parameters setup

The tests are carried out at both KTH and Swerim with same machining parameters and workpiece components except different CNC machines – SWEDTURN 300 (KTH) and OKUMA LB300-M (Swerim). The workpiece is S159 cylinder steel bar with length of 170 mm and diameter of 120 mm. there are six different types (S11, S12, S21, S22,

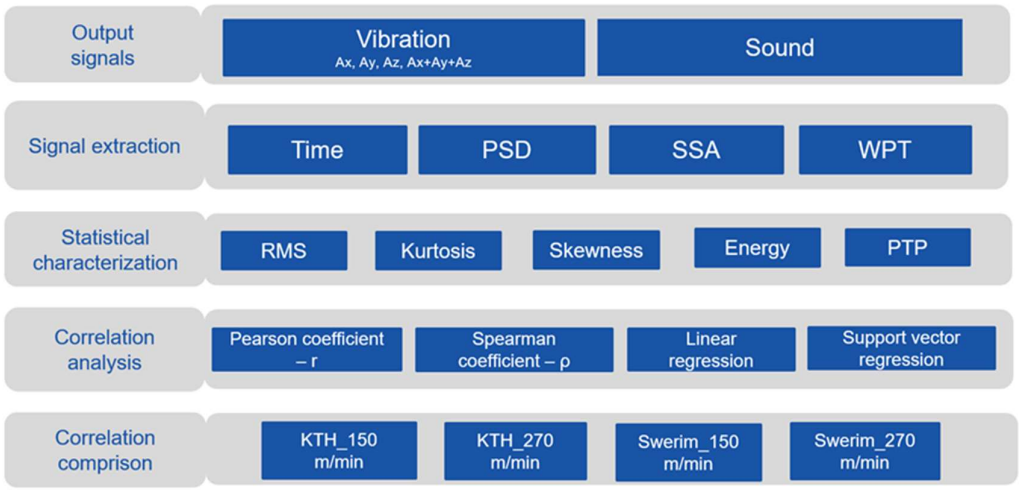

S31 and S32) and four workpiece of each types (totally 24 workpiece). For each type of workpiece, two of it are machined at low cutting speed (V_c = 150 m/min) and two others are machined at high cutting speed (V_c = 270 m/min). Each workpiece is machined by three runs with 165 mm cutting length of each run. And two same type workpiece are machined on the same cutting insert. Except the cutting speed, other cutting parameters such as feed (0.15 mm/rev) and depth of cut (0.1 mm) are fixed in all rounds. During each run, sound and vibration signal are captured and collected. After each run, the surface roughness is separately measured at two sampling areas with following measurement method. Due to S31 and S32 workpiece easily lead to the tool breakage and unstable cutting process, in this project, data collected from these two types workpiece are not taken into consideration.

5.5.4 Signal Processing and feature extraction

The first 20s and last 20s original vibration and sound signal are removed. The signal for calculating are captured two time sections separately located at SA1 and SA2. The capturing time of each sampling area are 20 s. Then the

captured vibration and sound signals in time domain within separated sampling areas (SA1 and SA2) are further processed and transformed with some signal processing methods (Figure 9) including time domain analysis (TDA), Fourier frequency transform (FFT), singular spectrum analysis (SSA) and wavelet packet transform (WPT). After applied by these four methods, post-processed signals are further characterized by statistical and non-statistical parameters (Table 6) which is regarded as process of signal feature extraction. Then these signal features are further evaluated how well they are correlated to those measured surface roughness parameters by methods including Person coefficient (r), Spearman coefficient (ρ) and determination coefficients (R^2) of prediction results from linear regression and support vector regression (SVR).

Figure 9: Procedure of signal processing, extraction and correlation calculation

Signal processing methods:

- Time domain analysis (TAD) is most commonly used signal processing method for monitoring surface finish, which just directly takes original amplitude values (g) in selected time section or sampling areas in certain time range (SA1 and SA2) (Figure 8) into analysis and relevant feature calculation.
- Power spectrum density (PSD) is the outcome of normalizing the signal amplitude from fast Fourier transformation by frequency range. The features are calculated from whole frequency range (Figure 10) and from four split sub-frequency ranges (Figure 11). The correlation between features from whole range and four sub-frequency ranges and surface roughness are analyzed separately then compared together.

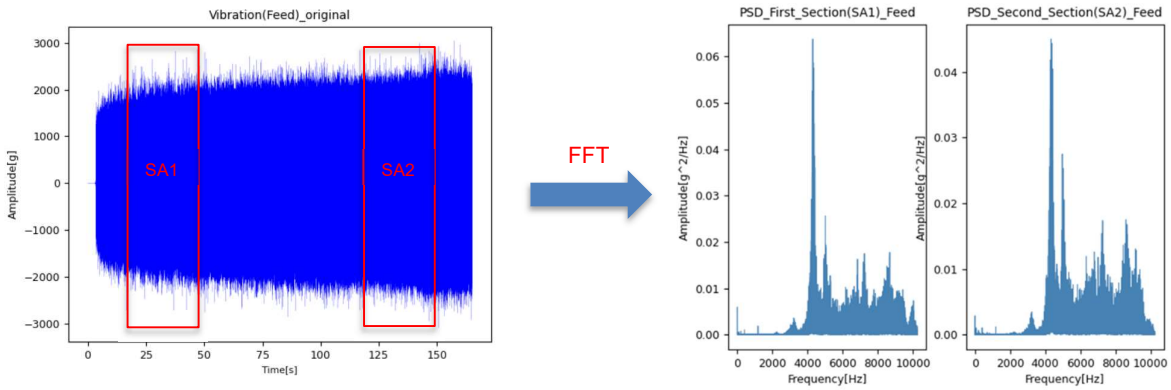

Figure 10: *Signal in time domain from SA1 and SA2 transformed into frequency domain*

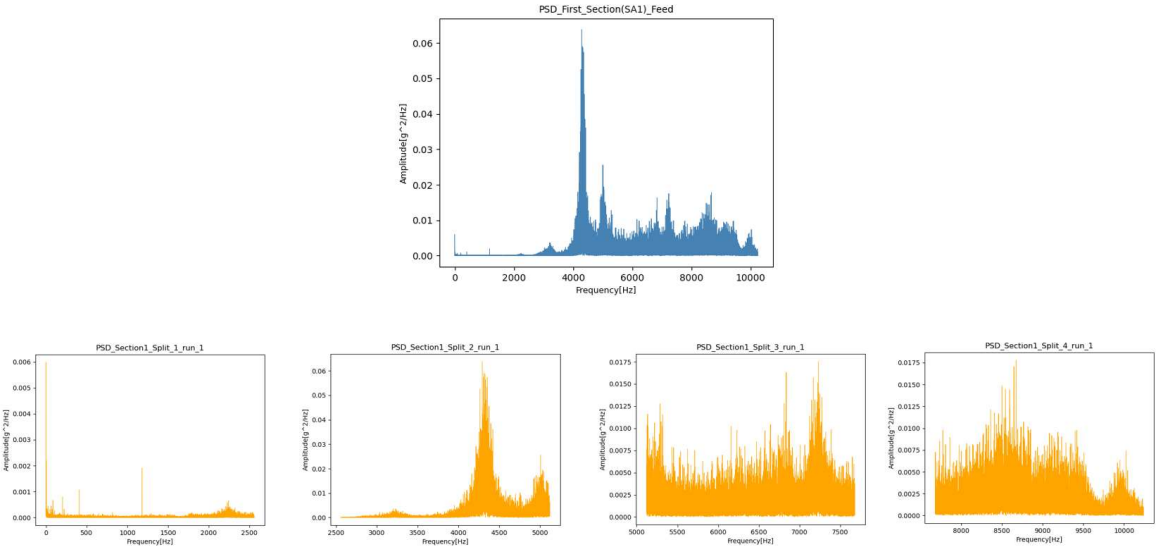

Figure 11: Signal in all frequency range and in decomposed sub-frequency (SA1)

- Singular spectrum analysis (SSA) is an advanced processing method on time series analysis and forecasting and focuses on singular value components of a specific matrix built on time series. SSA enables decompose the original series into small interpretable components explaining trend, oscillatory components and noise. The contribution of decomposed sub-component signals are calculated and those sub-component signals with high contribution percentages are selected for signal reconstruction (Figure 12). The two steps of SSA (decomposition and reconstruction) is a de-noising process where the unnecessary signal components are removed.

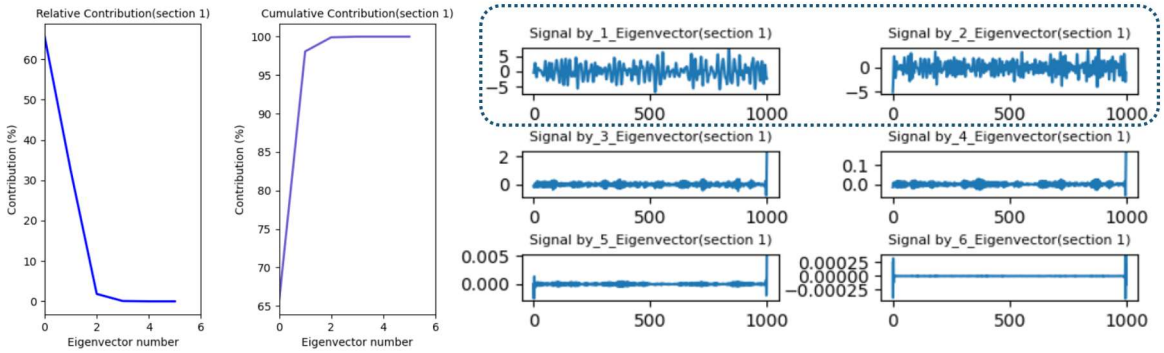

Figure 12: Contribution made by each eigenvector and signal based each eigenvector

- Compared with the short time Fourier transform, the wavelet packet transform (WPT) (Figure 13) can provide flexible resolution in time-frequency analysis based on different wavelet packet bases. The advantage of WPT is the decomposition of detailed signal in high frequency region. The signal reconstruction through decomposed signal selected by entropy or energy criteria. In this project, reconstruction depends on the energy of each decomposed signal and mother wavelets applied for vibration and sound signal are bior4.4 with 4 decompose level and coif4.4 with 5 decompose level respectively.

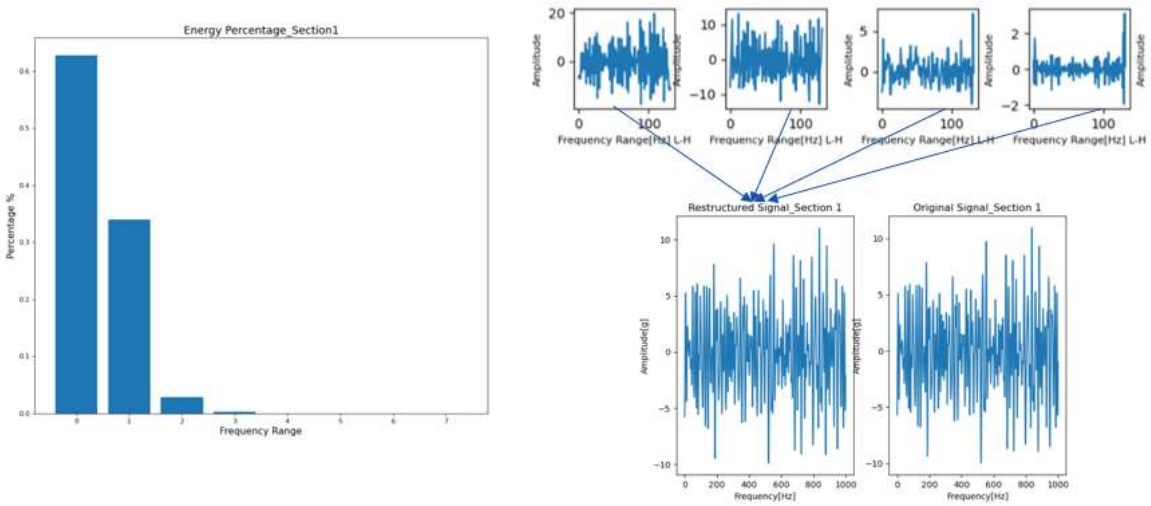

Figure 13: Contribution made by each eigenvector and signal based each eigenvector

Table 6: Signal characterization parameters

Features	Signal Features			
	ap	af	ac	sound
Standard deviation	STD_{ap}	STD_{af}	STD_{ac}	STD_{s}
Peak to peak	PTP_{ap}	PTP_{af}	PTP_{ac}	PTP_{s}
Skewness	S_{ap}	S_{af}	S_{ac}	S_{s}
Kurtosis	K_{ap}	K_{af}	K_{ac}	K_{s}
Energy	E_{ap}	E_{af}	E_{ac}	E_{s}
Shannon entropy	SE_{ap}	SE_{af}	SE_{ac}	SE_{s}

5.5.5 Correlation calculation and comparison

The correlation analysis is based on two correlation methods –Pearson (r) and spearman coefficients (ρ) and coefficient of determinations (r_2) from two surface roughness prediction models –multiply linear regression and support vector machine.

- Pearson coefficient is also referred to Pearson's r or the bivariate correlation is a statistical measurement evaluating the linear relationship between two continuous variables with the range between -1 and 1. The value of 1 represents complete positive linear correlation and 0 represents no any linear relationship.
- Spearman correlation assesses how well relationship between two continuous or ordinal variables by a monotonic function. The correlation calculation totally depends on the ranked values of each variable rather than the raw data.

5.5.6 Machine learning algorithm selection and implementation

Multiply linear regression (MLR)and support vector regression (SVR)are two most commonly used conventional machine learning algorithms. In this project, they are utilized for surface roughness prediction and final prediction result is further evaluated by the mean square error (er_2) and determination of coefficient (r_2) which can be also used for correlation measurement between surface roughness and each signal. Besides, the more advanced deep learning algorithm–multiply layers perceptron (MLP) are also applied into the prediction of final surface roughness. And its predicted results are further compared with results from two conventional algorithms respectively. Besides, the 3 folds cross-validation is implemented for algorithm training and prediction accuracy of surface roughness validating, in which the average values of prediction accuracy in three recursive runs from each algorithm are regarded as criteria of comparing performances among each trained algorithm and selecting the best hyperparameters for each algorithm to ensure the implementation of highest prediction accuracy.

- Multiply linear regression (MLR) in which multiply independent variables involves enables to build the hyperplane compared with independent linear regression which can only depicting the signal linear correlation. However, the MLR shares the same theory with independent linear regression. Both of them is based on the theory of minimizing the error between target values and predicted values. In this project, the multiply linear regression is applied to correlate the multiply variables-features extracted from signal in different domains to surface roughness (R_a)as final predicted results or outputs.
- Support vector regression (SVR) has totally different algorithm theory with multiply linear regression (MLR), which aims to fit the best line with a threshold value with its unique kernel functions in form of linear, sigmoid, polynomial and radial basic function (RBF). To be more robust to outliers with, SVR processes the capacity of excellent generalization and high prediction accuracy when there is the small amount of sample data. In this case, the SVR (gamma = 0.04 and epsilon = 0.01) with kernel function of RBF get involved into the implementation of surface roughness prediction.
- Multiply layer perceptron (MLP) aka. Artificial neural network (ANN) is one of supervised learning algorithm, which consists of one input layer, one output layer and one or more hidden layers. And each layer is composed of some nodes in which nonlinear activation functions such as ReLU, sigmoid and tanh are located to describe the nonlinear relationship between layers. To select activation function, number of hidden layers and number of nodes in each layer as process of hyperparameters tuning totally depends on amount and characteristics of data. There is no rule of thumb to make this process consistent. In light to the tests, in this case, MLP with best prediction performances (highest prediction accuracy) includes its layer structure 15-10-6, sigmoid as activation function and scholastic gradient decent (SGD)as solver.

6 Results and Discussion

6.1 Heat treatment - Carbon content

Was measured on test rods cut from the larger lab components as seen in Figure 14 and Figure 15. The simulated carbon content from recipe design agrees well with experimental results, see Table 4. It can be noted that there is an increase of carbon content below 0,2-0,5 mm due to the boost-diffusion concept.

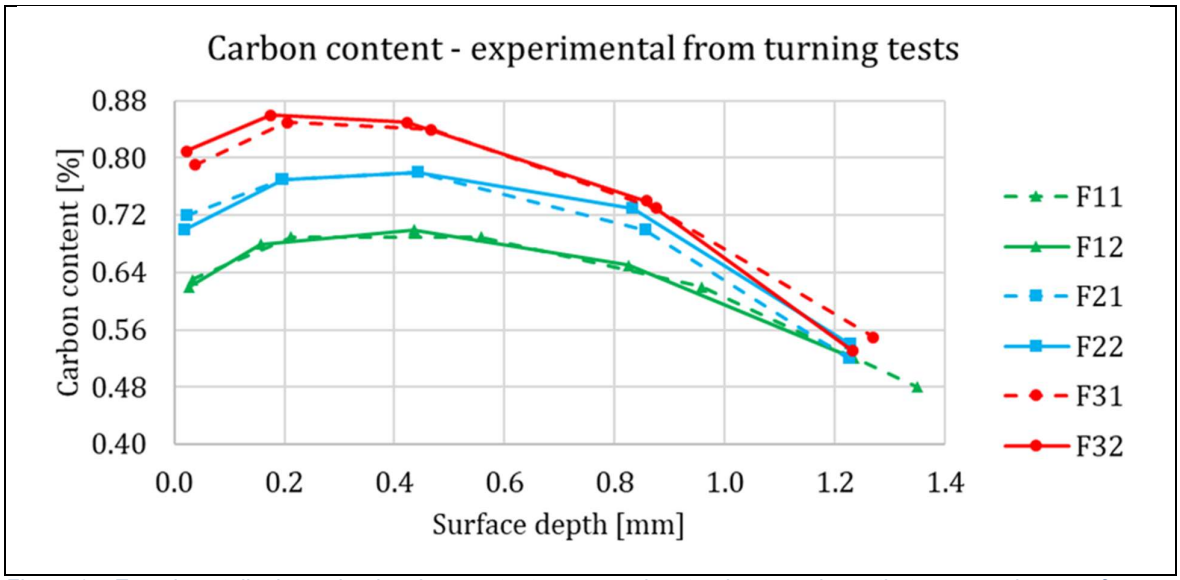

Figure 14: Experimentally determined carbon content, measured on turning test-pieces that were run in every furnace batch. These results are from the furnace batches with Ovako 236F tubes.

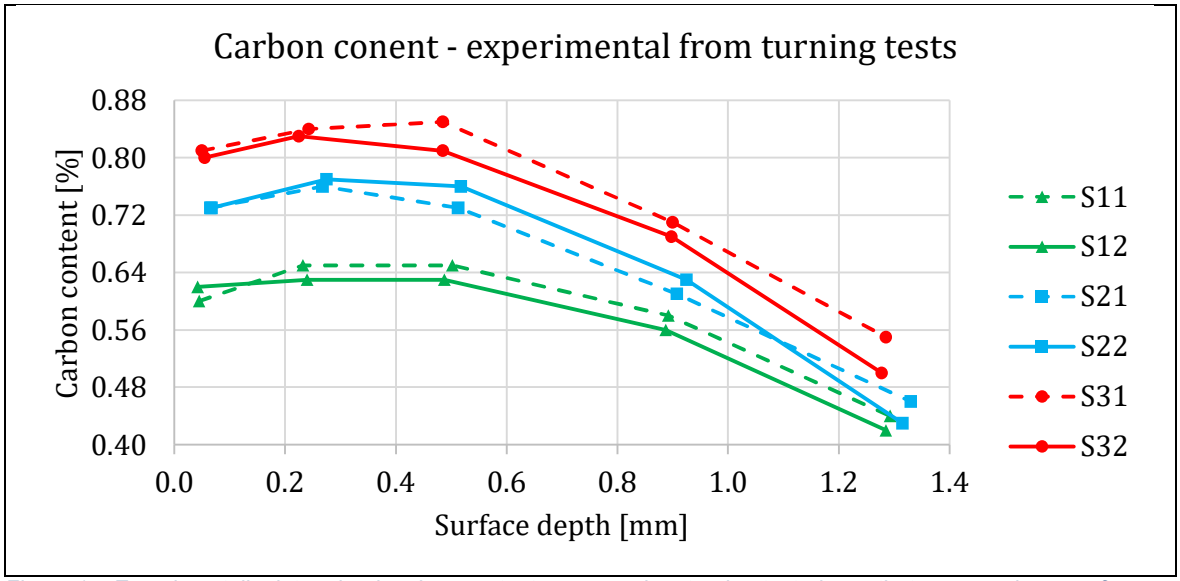

Figure 15: Experimentally determined carbon content, measured on turning test-pieces that were run in every furnace batch. These results are from the furnace batches with Ovako 159S tubes.

6.2 Charaterization of hardness, retained austenite and microstructures

Labcomponents used in machining tests were characterized by hardness retained austenite and light optical microscopy. The results from the hardness measurements as seen from Figure 16 and Figure 17, and can be summarized as follows:

- Surface hardness is above 700 HV1 for all series except S31 and S32, which is probably due to high retained austenite content.
- Case depths are approximately 1.5-1.7 mm for all series.
- The resulting matrix is within common production specifications for transmission components.
- The carbon content and the hardness measurements agree well.

Specifically for the two steel grades:

Ovako 236F
- Similar hardness profiles for tempering at 180°C.
- Tempering at 160°C seems to affect 0.64 series less, when compared to 0.72 and 0.80 series.

Ovako 159S
- Similar hardness profiles for 0.64 and 0.72 series test-bars (S1X, S2X).
- Clear tempering effect for 0.64 and 0.72 series test-bars (S12, S22).
- Low surface hardness for 0.80 series (S31, S32).
- Tempering effect less pronounced for 0.80 series (S31, S32).

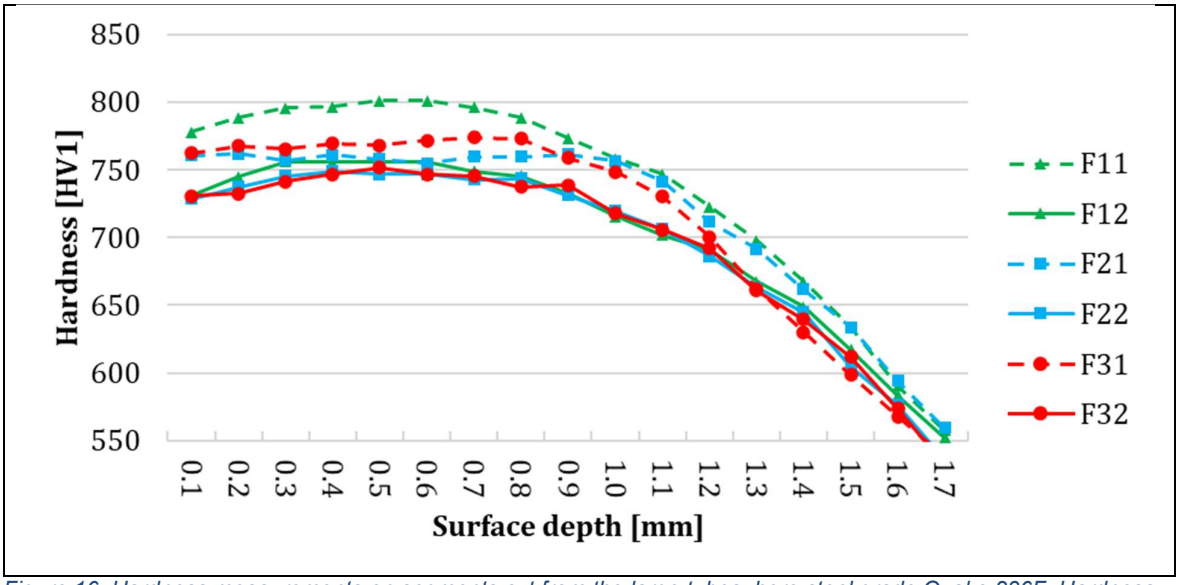

Figure 16: Hardness measurements on segments cut from the large tubes, here steel grade Ovako 236F. Hardness is given as average values from three measured profiles.

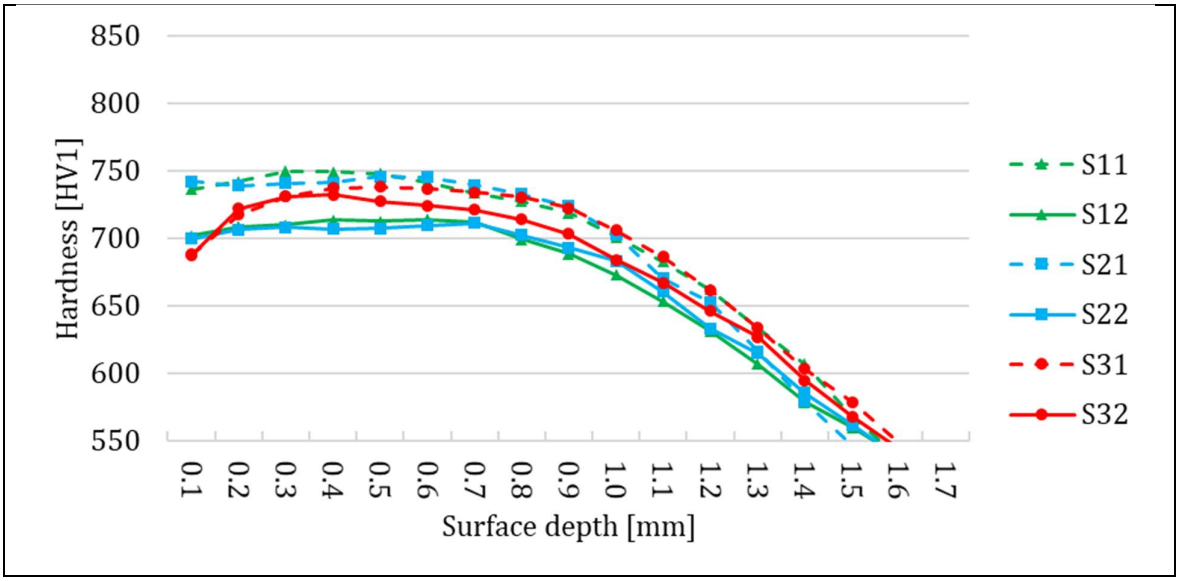

Figure 17: Hardness measurements on segments cut from the large tubes, here steel grade Ovako 159S. Hardness is given as average values from three measured profiles.

The results from the retained austenite measurements (Figure 18 and Figure 19) were summarized as follows:

Ovako 236F

- Similar retained austenite content for 0.72 and 0.80 series.
- 0.64 series shows a lower retained austenite content in comparison.
- No obvious effect by tempering on the retained austenite content.
- Low value for 20 µm measurement of F32 is probably due to HTTP.

Ovako 159S

- Clear shift in amounts of retained austenite with carbon content.
- No obvious effect by tempering on the retained austenite content.
- Low value for 20 µm measurement of S32 is probably due to HTTP.

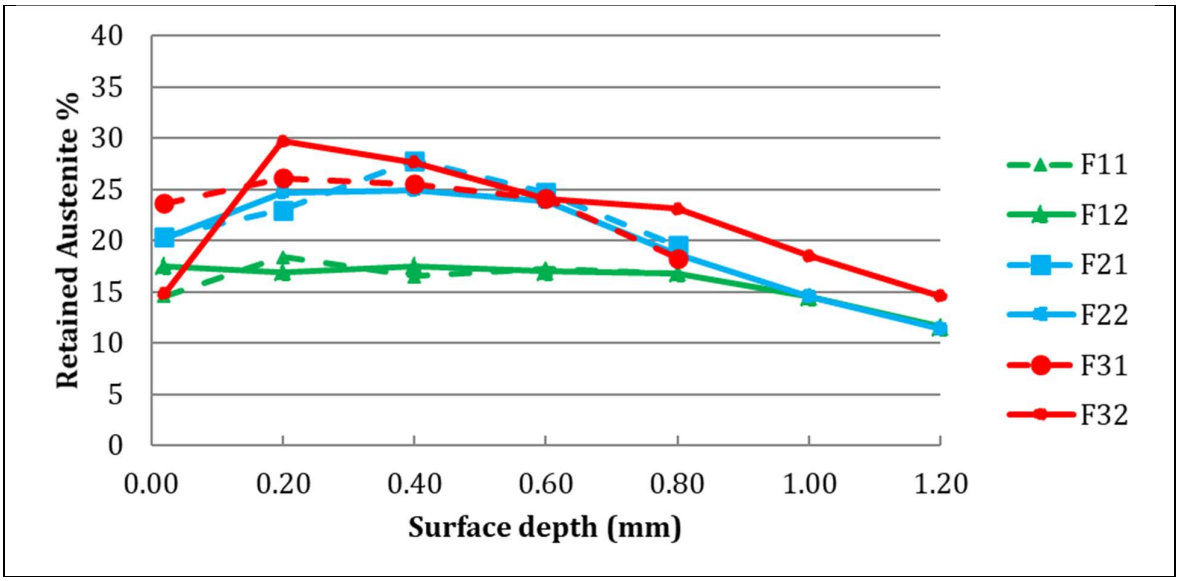

Figure 18: Retained austenite measured on case-carburized tubes after hardening, here steel grade Ovako 236F.

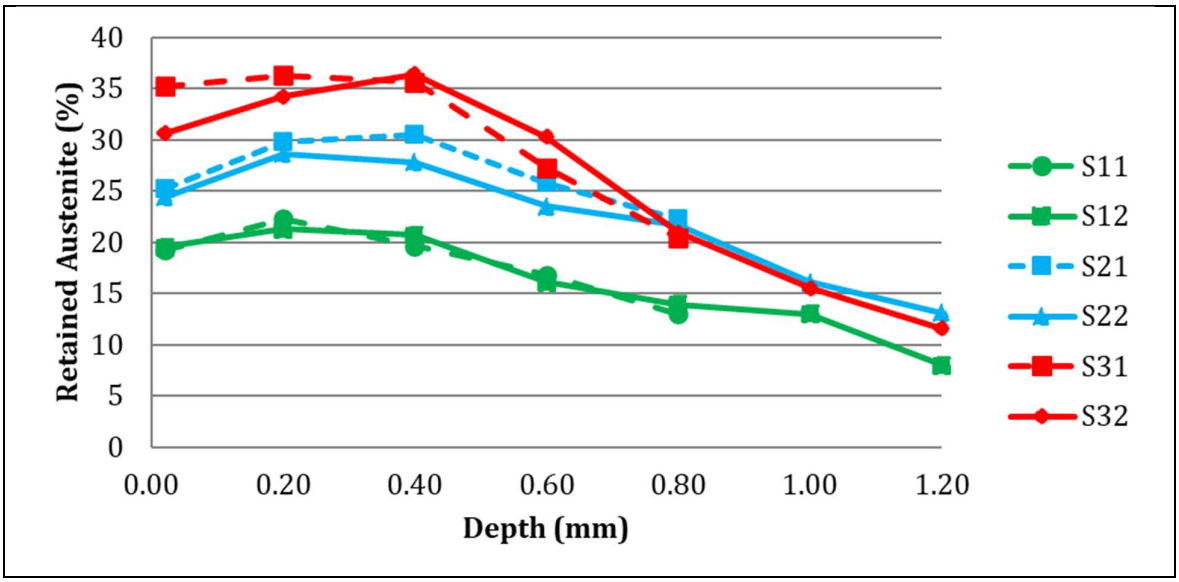

Figure 19: Retained austenite measured on case-carburized tubes after hardening, here steel grade Ovako 159S.

Results from the light optical micrographs:

As seen in Figure 20 and Figure 21, higher fraction of retained austenite and high-carbon plate martensite is present in samples carburized at higher Cp. In contrast, low Cp (0.6) display low-carbon lath martensite and less RA. This is especially visible when comparing Cp 0.6 to Cp 0.73. Further increase is not as clear when comparing Cp 0.73 to Cp 0.8. In S31 the etching was slightly weaker.

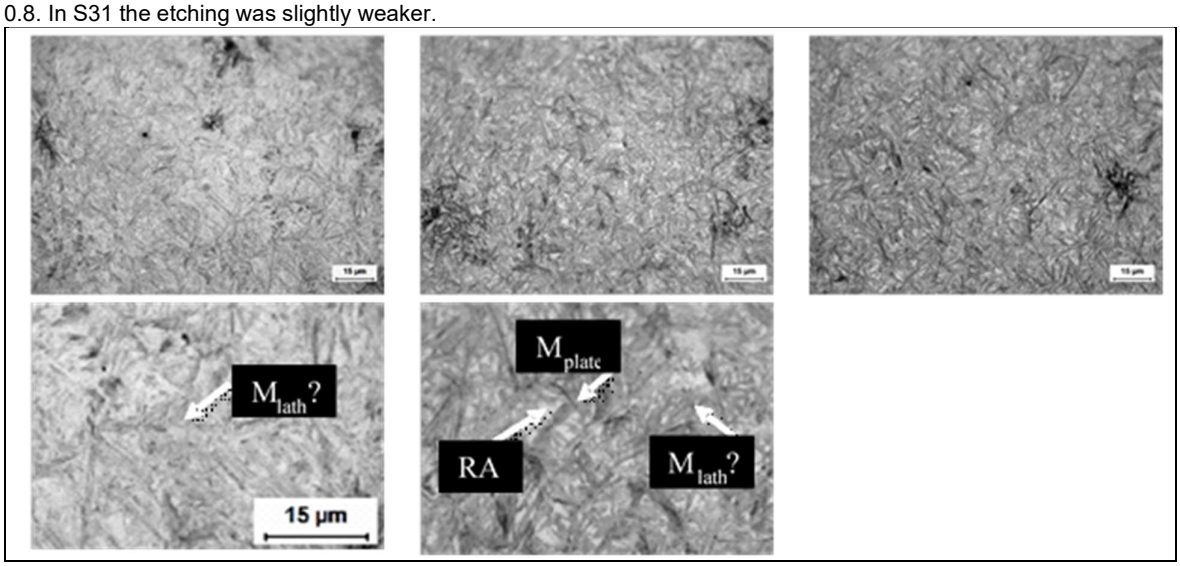

Figure 20: Cross section microstructure of F-steel (16MnCr5) after case hardening, tempered at 160°C. fLTR: F11, F21, F31. Images captured at 200 µm distance from surface. Arrows highlight the various phases, identifiable by their shape and colour.

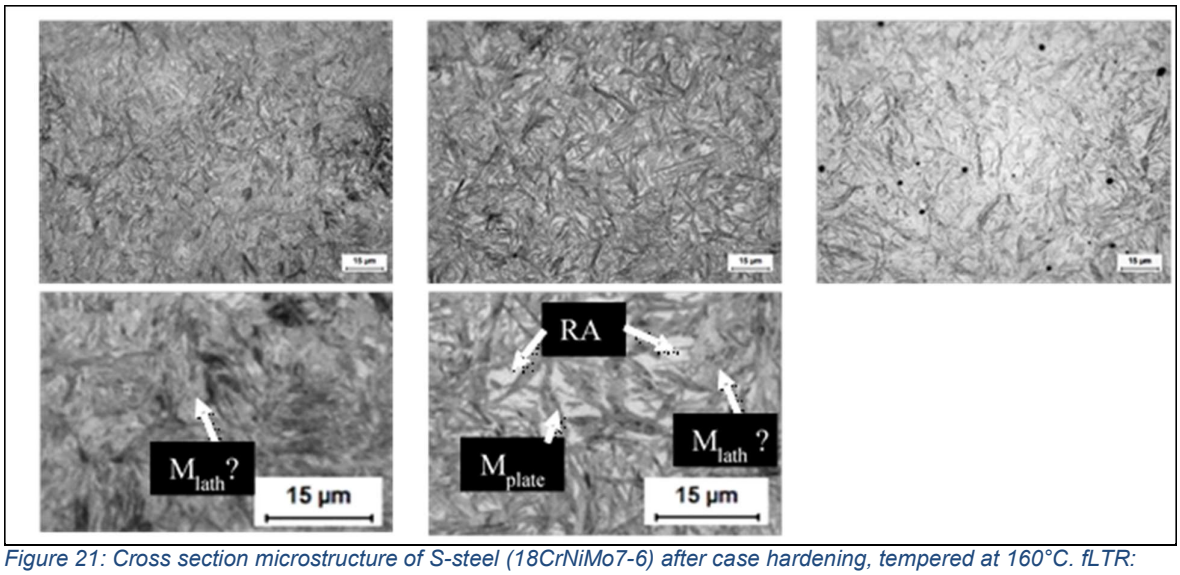

Figure 21: Cross section microstructure of S-steel (18CrNiMo7-6) after case hardening, tempered at 160°C. fLTR: S11, S21, S31. Images captured at 200 µm distance from surface Arrows highlight the various phases, identifiable by their shape and colour.

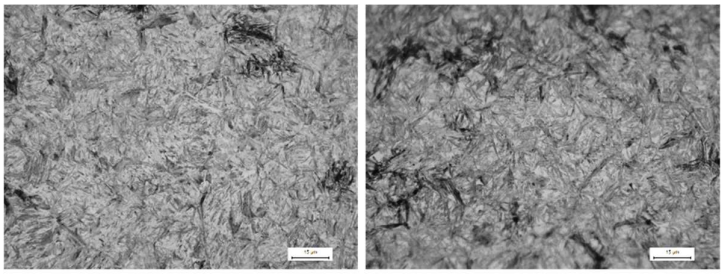

Figure 22: Cross section microstructure of F-steel (16MnCr5) after case hardening, tempered at 180°C. fLTR: F12, F22. Images captured at 200 µm distance from surface.

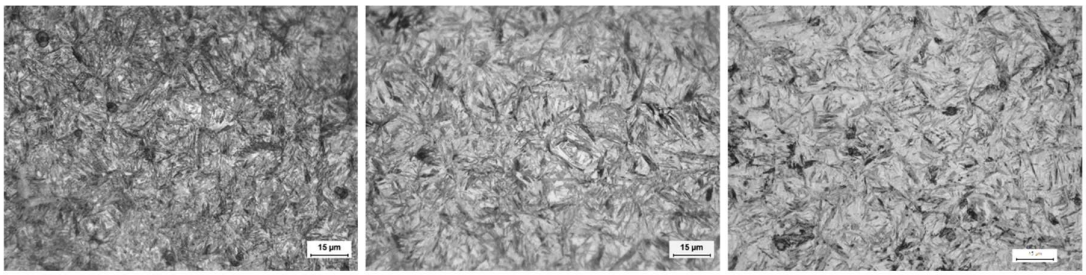

Figure 23: Cross section microstructure of S-steel (18CrNiMo7-6) after case hardening, tempered at 180°C. fLTR: S12, S22, S32. Images captured at 200 µm distance from surface.

All samples display non-martensitic transformation products (i.e. high temperature transformation products, HTTP) in first couple of microns. For higher alloyed S-steel, HTTP reaches up to 10 µm depth, while lower alloyed F-steel it reaches up to 25 µm. This is exemplified in Figure 24.

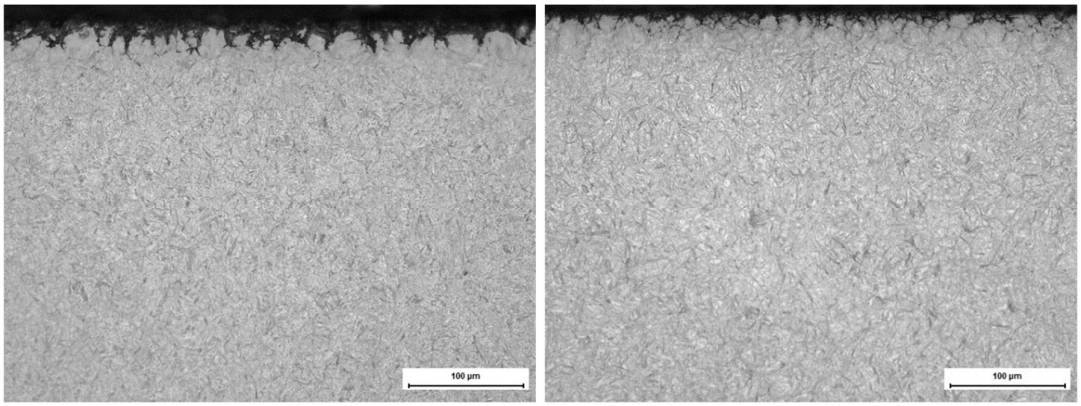

Figure 24: Cross section of the near-surface region of F21 and S21 after case hardening. HTTP is visible as dark at a depth of 10-25 µm.

6.3 Machining and Tool wear studies

As outlined in Figure 25, several test setups were run on the same types of test parts. These tests will be discussed here in different combinations:

- The different steel types (S and F)
- Wear types (flank wear, crater wear) in relation to material characteristics (hardness and residual austenite) or hardening variables (% C, tempering temperature)
- Phenomenological (**6.3.1**) and production like (**6.3.2**) tool wear

Figure 25 shows the hardness and residual austenite of the different steels (F steel, left, S steel right), grouped into “main variants” with properties in a narrow range (dashed) and extremes (marked with solid circles).

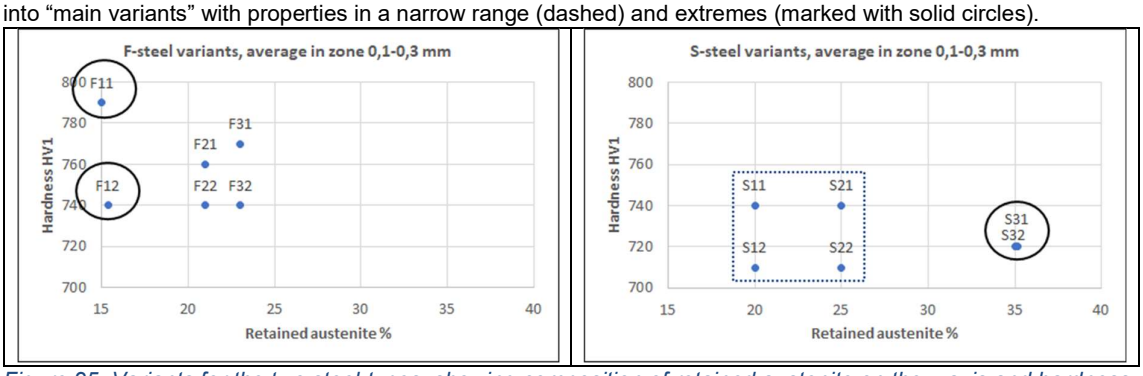

Figure 25: Variants for the two steel-types, showing composition of retained austenite on the x-axis and hardness on the y-axis. Steel-variants 236F in left panel and 159S in right panel. Sub-groups of extreme variants (solid) and separately compared variants (dashed) are marked.

The inserts show a wear pattern typical for cBN inserts in Hard Part Turning, with flank wear, crater wear and some tendencies to notch wear. For anyone familiar with inserts from soft machining, it should be noted that the wear zone is small, related to the small depth of cut. In Figure 26 (left), an insert in cutting is shown (from Coromant marketing material), where it is demonstrated that the depth of cut is smaller than the nose radius. A top-view image of a worn insert (middle) shows the corresponding wear pattern (note however opposite direction compared to the cutting in the left image), localized on one side of the nose. An SEM image of the actual wear region is shown in the right-most picture, including wear denominations.

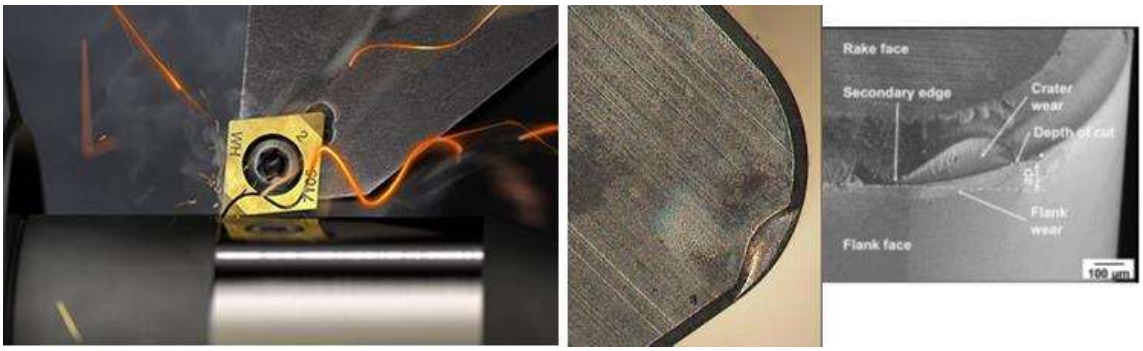

Figure 26: Left: insert in machining (from Coromant marketing material), middle: top-view of worn insert, right: wear seen in SEM, from Ånmark 2015 [4].

On an overall level, Figure 27 and Figure 28 show measured wear for the different tests sets. The complexity of the data sets is obvious and hinders deeper understanding. For more conclusions, data will need to be looked at in different perspectives. From this overview, two main effects can however be seen:

- Cutting speed has a major impact on wear, both flank wear and crater wear (note different scales used for the different speeds).
- In many cases, the S steel shows more wear than the F steel, in particular crater wear and more pronounced at the higher speed. This does not hold true in each data point however, and needs to be

looked at in more detailed analysis, in particular the split between finishing (phenomenological) and roughing (production-like) setups.

In terms of relations of wear versus hardening parameters, no overall trends can be seen, and it cannot be said that carbon potential or tempering has the dominating effect. Instead, there appears to be an interplay between these, that requires further analysis in sub-sets.

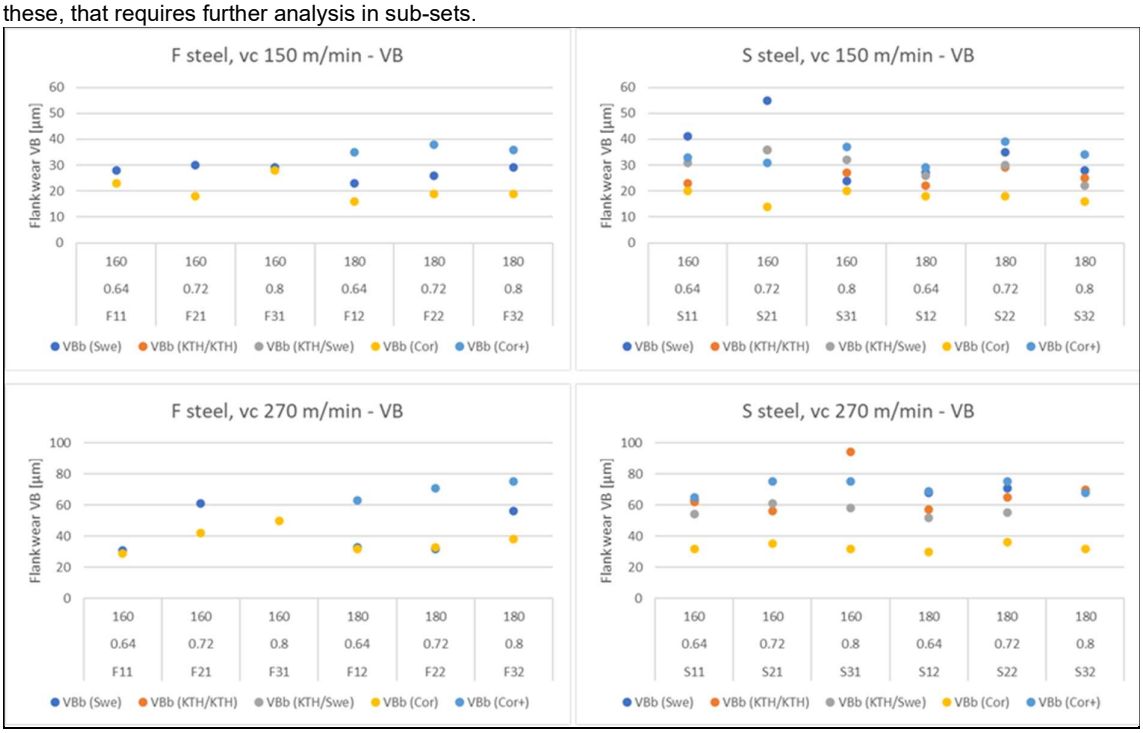

Figure 27: Overall wear plots, flank wear (VB). For different steels (F steel left, S steel right) and cutting speeds (150 m/min upper, 270 m/min below). Each plot including the different test sets as data series, and the different hardening conditions (C% and tempering temperature) on x axis.

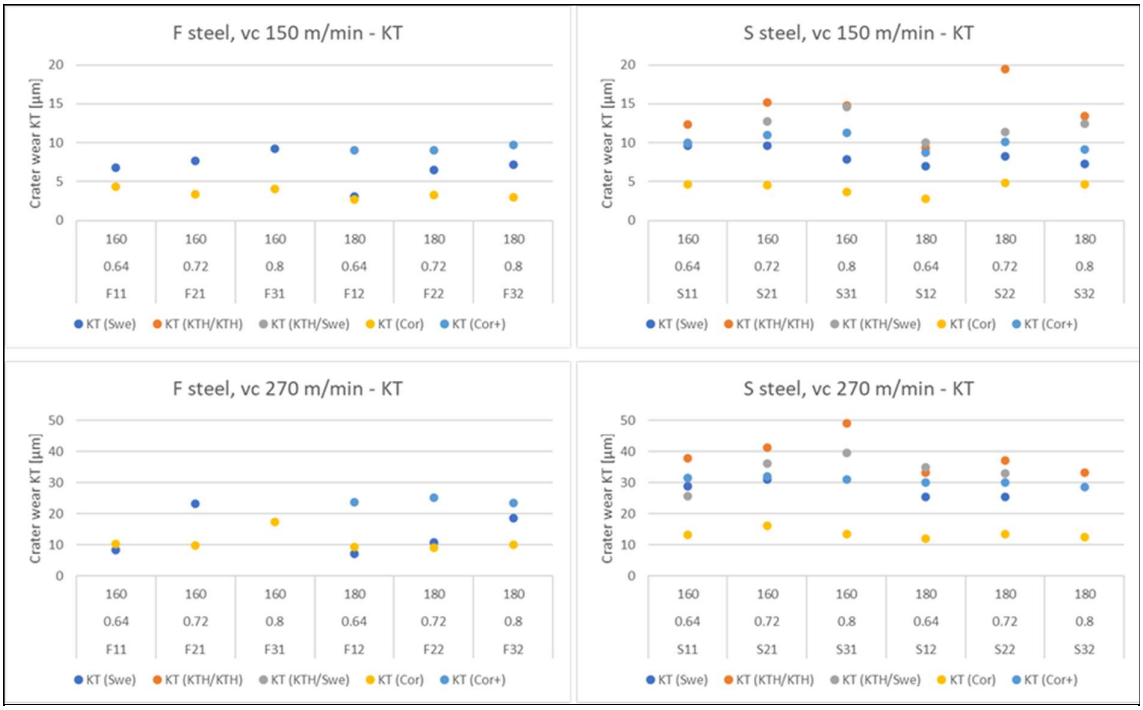

Figure 28: Overall wear plots, crater wear depth (KT) Diagram structure and layout same as above.

For a sub-set of data, focused on the S steel at the lower cutting speed, vc 150 m/min, Figure 29 and Figure 30 show flank and crater wear respectively. This data is separated on tempering temperatures (T 160, variants Sx1) to the left, temperature 180 (Sx2) to the right. Within each group, there is a tendency to a negative optimum, with more wear at the average C%. This trend is valid over the different test setups (COR/KTH/SWE…).

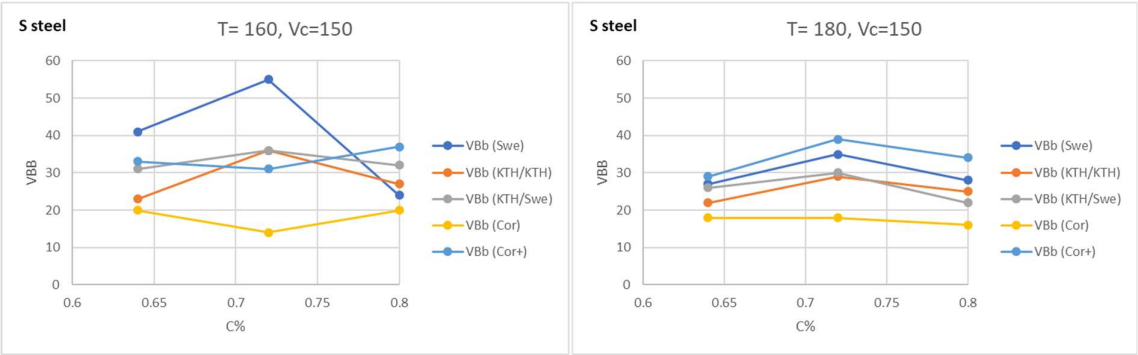

Figure 29: Wear plots, flank wear VBB [µm] for sub-set S steel at vc 150 m/min; left: variants at tempering T 160 degrees (variants Sx1)), right: 180 degrees (variantsSx2))

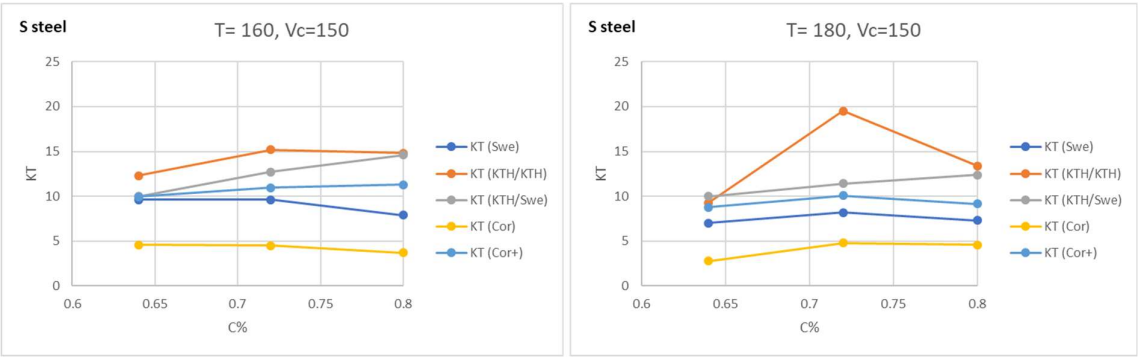

Figure 30: Wear plots, crater wear KT [µm] for same sub-set of variants as above

In Figure 31, wear (flank and crater) is plotted versus hardness. (As opposed to Figure 29 and Figure 30, these are plotted for the full datasets, including all combinations of %C and tempering). There are no apparent trends.

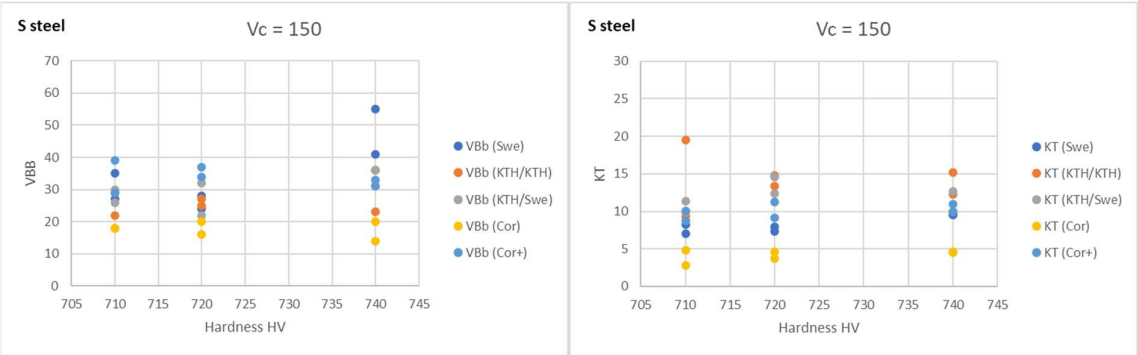

Figure 31: Wear (flank wear VBB, left and crater wear KT right) versus hardness HV, for all data sets of S steel at vc 150 m/min

In several test setups, surface generation was measured over time. No significant differences or trends could be seen that can be related to the hardening variants. See however separate note under section 6.3.1.

In summary, the overall wear analysis points at some trends, but further analysis will be needed in the different sub-sets below.

6.3.1 Phenomenological tool wear, influence from material

In test package COR, short tests were run (CCL approximately 880 meters, see Table 5) for comparison of different zones. Wear was evaluated qualitatively (SEM images) for all edges, and numerically for edges run in zone 2.

The main result in this part, is the significant difference in appearance for edges run in zone 1, the clean cut, versus the cuts deeper into the material (zone 2 and 3). An example is given in Figure 32, for steel / hardening variant S11 at cutting speed 210 m/min. Wear for edges run in zone 2 (middle) and 3 (right) is limited and showing the same appearance with minor differences. For the left-most edge, run in zone 1, wear is both more pronounced and larger in size. The larger wear mark indicates on a depth of cut larger than anticipated, in turn related to run-out of the parts. The degree of wear related to run-out varies between tested edges, indicating a variation in the degree of run-out between parts and possibly steel grades (more run-out for S steel, see discussion in 6.3.2).

Secondary to the differences seen for zone 1, there is an indication on less wear in zone 3 compared to zone 2. Due to the limited amount of wear, no details can be concluded on the relative wear in these zones for different materials. For the remainder of this work, it is estimated safe to combine zones 2 and 3 for wear investigations, whereas zone 1 stands out due to large scatter.

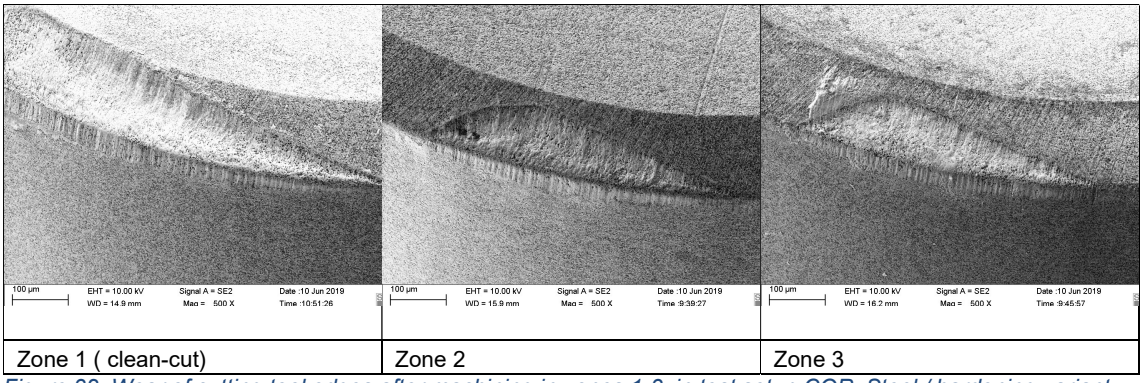

Figure 32: Wear of cutting tool edges after machining in zones 1-3, in test setup COR. Steel / hardening variant S11, cutting speed 210 m/min. Note difference in wear mark size, extending to the left of the picture for Zone 1.

For zone 2, wear was evaluated also numerically. The amount of wear is however very small, with crater wear depth KT < 20 µm and flank wear width VBB < 50 µm. For the impact of steel / hardening variations on wear, more focus is therefore given to the longer test package COR+.

The test package COR+ denotes the longer-time test. It has been run in 4 cuts, thus including zones 2 and 3, but not the outermost skin of zone 1. Wear was evaluated numerically. Flank wear VBB and crater wear depth KT are shown, plotted against material parameters of the hardened steel, in Figure 33and Figure 34, both for the S steel at 270 m/min. While it is clear from these plots that hardness (HV) alone cannot explain the variations in wear between hardening variants, trends are not straight-forward. For the relation to RA, there would appear to be a maximum in wear at average RA values. Such relations would suggest that different mechanisms come into play, where some mechanism creates an increased wear rate with increased residual austenite, whereas some other mechanism causes a reduction.

While these data series are based on single edges run per test condition, thus not taking any scatter into account, it should be noted that similar trends are seen in the majority of 6 independent data sets; combining shorter and longer tests (COR and COR+) at three different cutting data (150, 210 and 270 m/min), providing support for the trend. (Data for vc 150 and 270 can be seen in Figure 27 and Figure 28). In addition, see discussion around Figure 29 and Figure 30, where the same trend was seen over the different test sites.

A selection of the dataset COR+ at cutting speed 210 m/min, was also basis for [Boing et al. (2021)[8]] Variants S11, S12, S21 and S22 were selected for that work, based on their pair-wise data in hardness and residual austenite, thus possibility to compare the relative effect of these parameters. In that work, clear trends were shown, an increased wear by both RA and HV. As seen here, that trend is not valid over a broader spectrum of material characteristics. In particular, it can be noted that the high RA variants S31, S32, do not show more pronounced wear.

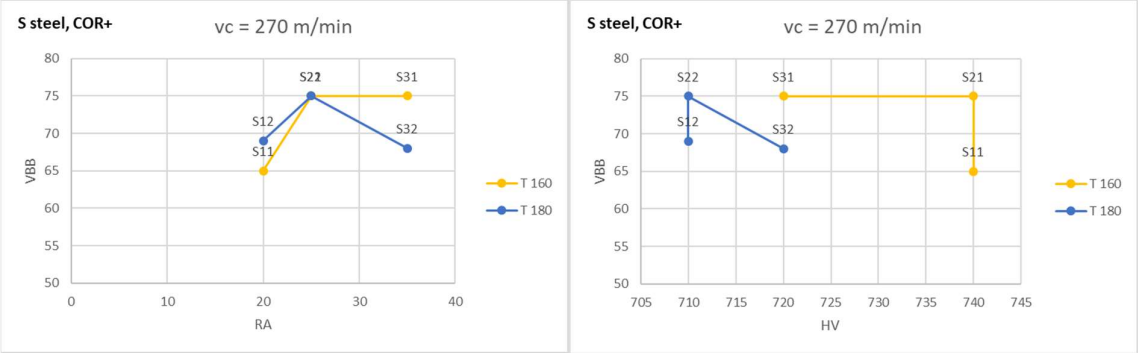

Figure 33: Plots of flank wear width VBB versus steel characteristics HV and RA, for steel S at cutting speed 270 m/min

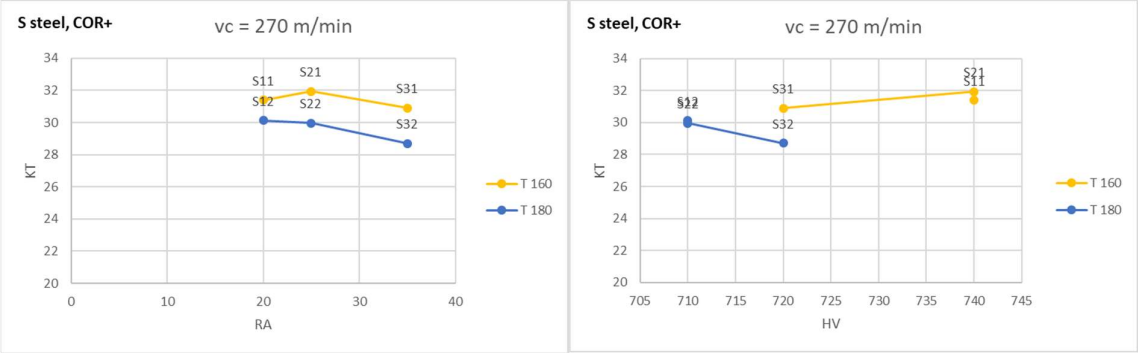

Figure 34: Plots of crater wear depth KT versus steel characteristics HV and RA, for steel S at cutting speed 270 m/min

Translated to industrial applications, the indication that wear depends on residual austenite, but not in a linear way, would imply that

- In a given process, variations in workpiece material and hardening processes (by intentional variations or scatter) can impact on the machining process by wear and tool life,
- This may give room for optimizations of machining, both by process adjustments and by narrowing of process windows.
- However, it is difficult to establish guidelines, as no simple overall trends are seen.
- (Furthermore, it must be noted that this investigation has covered continuous wear types only, not looking into effects on eg. adhesive or mechanical wear.)

In Figure 35 and
Figure 36, crater wear (KT) and flank wear (VB) are shown versus measured residual austenite for steels S and F. The S steel is here shown to have generated more crater wear (Figure 35) at a given level of residual austenite. Note that variants with enlarged markers have similar hardness, thus isolating effects of steel type and residual austenite. The role of the steel type is larger than that of residual austenite within each steel.

The same difference cannot be seen at lower speed (data not isolated here, see instead upper row of Figure 28, where variants have the same level of wear in test COR+). This indicates on a temperature driven mechanism, thus enhanced at higher cutting speed. The steel difference is not seen for flank wear (
Figure 36), possibly due to the fact that flank temperatures are lower and wear less chemically driven.

For industrial applications, where applicable, the selection of steel type may thus be more important than the hardening variables, to design a process with given level of residual austenite and hardness, yet controlled machinability, in particular at increased cutting speed.

This may be an important contribution to understanding, in reference to previous work [Björk et. al.[6]], where machinability of different steels in hard part turning were addressed but could not be safely concluded due to variations in hardening outcome. At controlled hardening, the impact of steel grades can now be concluded.

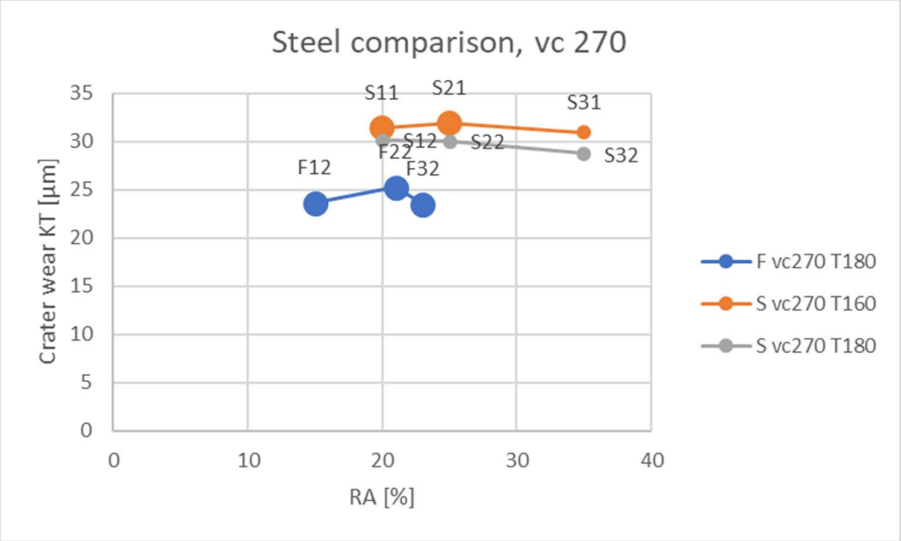

Figure 35: Comparison of crater wear (KT) for the two steels, at cutting speed vc 270

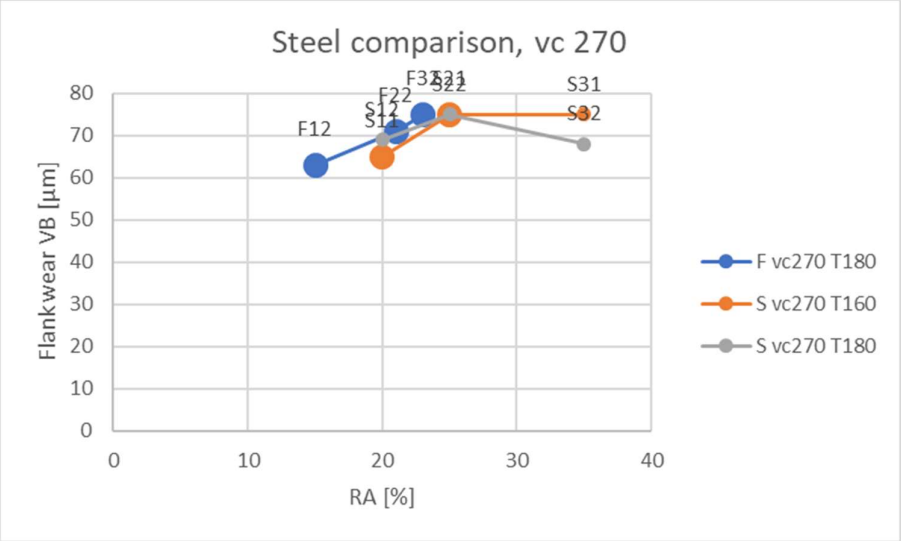

Figure 36: Comparison of flank wear (VB) for the two steels, at cutting speed vc 270

Generated surface, plotted over machining time, is shown in Figure 37. At vc 150 m/minutes (solid lines in each diagram), no significant difference can be seen between the F and the S steel, or between hardening variants of one same steel. At increased cutting speed, 270 m/min (dashed lines), both steels generate lower surface roughness values compared to vc 150 m/min. This effect is small for the S steel, but pronounced for the F steel.

Cutting speed and steel grade are critical here, whereas hardening variables do not appear critical for surface generation in these conditions.

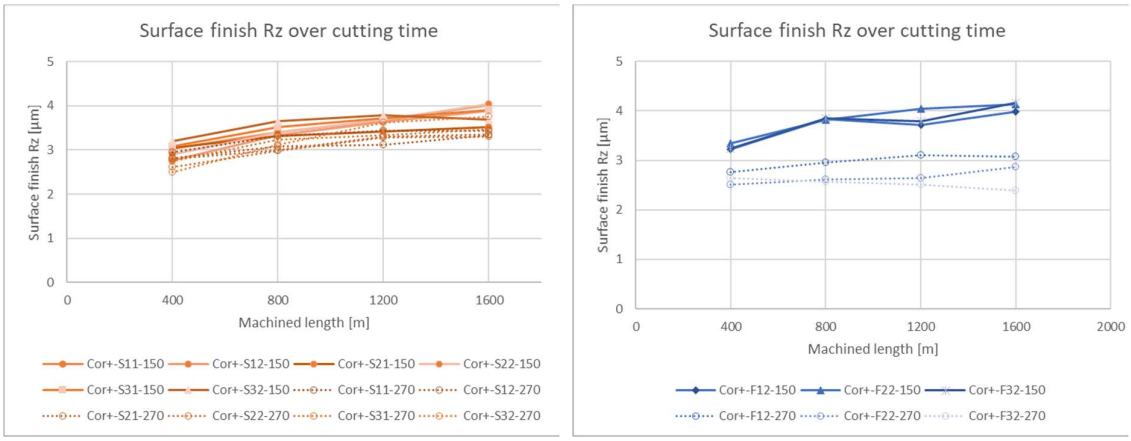

Figure 37: Surface roughness Rz over cutting time. Left: S steel. Right: F steel. Both showing two sets of cutting data, with vc 150 m/min shown as solid lines, vc 270 m/min as dashed lines.

6.3.2 Production like tool wear, influence from material and system set-up

Machining in zone 1 and 2 result in complex tool wear, including a double crater due to the first clean cut in the surface with dimensional variation, creating a variable cutting depth. The degree of different run out seen between the steel grades may be related to the higher distortion potential in the S-steel, which could imply that failures are not related to the material / wear relations as such, but to different load situations at varying depth of cut. Figure 38 is showing tool wear in the two different steels having virtually the same harness and retained austenite. These results are based on single edge tests, repeated twice in the same lathe (SWE and KTH-SWE) and once in another lathe (KTH-KTH). The representation of data is based on general trends and similarities within and between the tests. The KTH - tests were also intended for the robustness test reported in **6.4**.

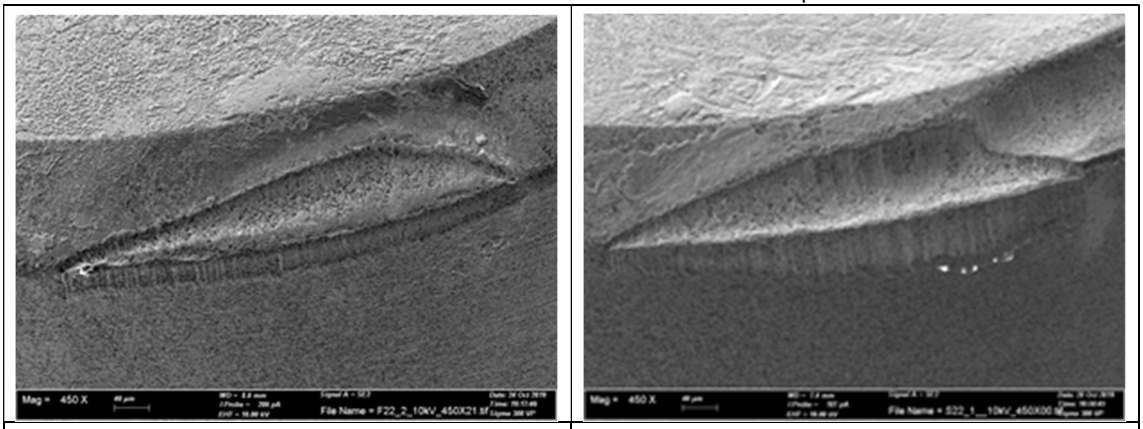

F22 ~ RA 20%, 740 HV1	S11~ RA 20%, 740 HV1

Figure 38: showing the double crater from machining in zone 1 and zone 2 in two different steels with virtually the same hardness and retianed austenite, run at 270 m/min.

Some tested edges have shown edge chipping or breakages. It is notable that variants S31 and S32 showed multiple such occasions, i.e. SWE, SWE-KTH, KTH-KTH tests, possibly indicating an effect of the high residual austenite (~35 %) of these variants. All failures occurred at the higher cutting speed (270 m/min). No failures were seen for the F steel. While this may also be related to other differences, it is worth noting that the F steel did not reach the same levels of residual austenite.

Trends were seen between variants with large deviating properties (F11/F12) and (S31/S32) or between variants where eg.hardness or retained austenite varied (S12/S11/S22/S21), see Figure 25

The results for flank wear, crater wear or notch wear is not showing a strong trend within the window of variants, although comparing F11/F12 with the higher carburized variants, we can see a slight trend of increase flank and crater wear with increasing carbon, corresponding to an increase in retained austenite. Figure 39.

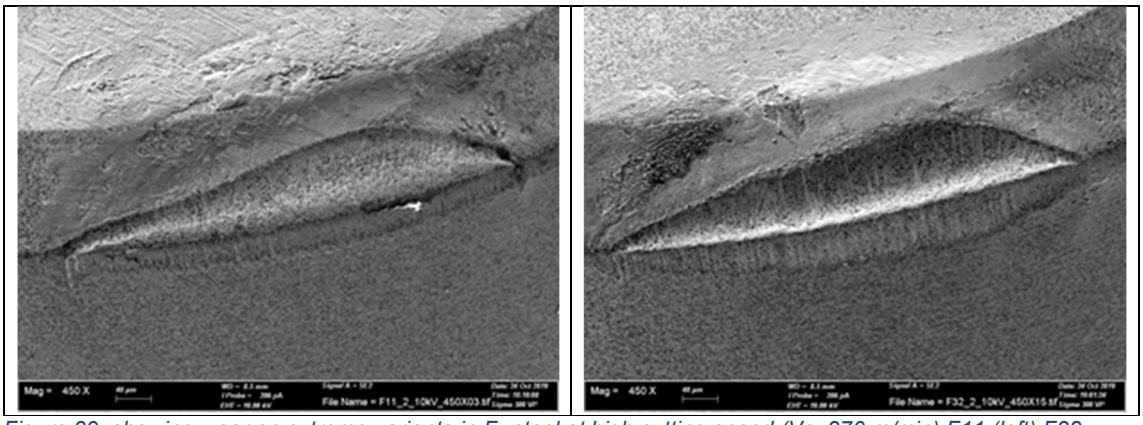

Figure 39: showing wear on extreme variants in F--steel at high cutting speed (Vc=270 m/min) F11 (left) F32 (right)

Looking at numerical tool wear, shown in Figure 40, hardness do not drive wear (right panels). The left panels showing that crater wear and possibly also flank wear increase at increased amount of retained austenite. Note the lesser span of retained austenite between the 0,72 and 0,80 series, compared to S-steel, due to carbon saturation. At higher cutting speed, higher temperature accelerates reaction rates causing increased wear [Boing et al.[8]] – and thus stronger relations versus retained austenite. It must also be noted that results may also be affected by scatter artefacts in the outer scale.

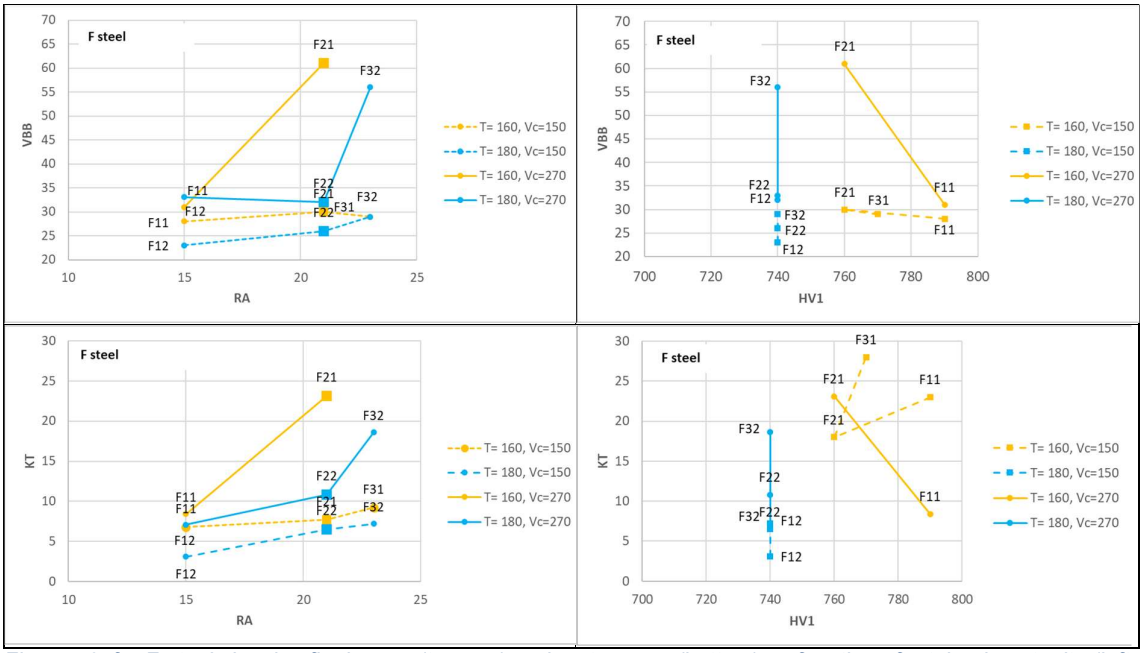

Figure 40, for F-steel showing flank wear (top row) and crater wear (bottom) as function of retained austenite (left panels) and hardness (right panels)

The matrix of S-steel variants represented a span of retained austenite and hardness. At the highest level of retained austenite the hardness is the same for the two variants. As seen in Figure 41, tool failure occurred for

variants S31 and S32 at high cutting speed, the same was seen in the other set-ups. The S21-variant also shows failure in Figure 41, but only in this set-up. Variants S31 and S32 have the highest amount of retained austenite while S21 has a combination of high hardness and relatively high amount of retained austenite. It is suggested that the combination of high hardness and high amount of retained austenite may be fatal for tool life. For S21 this was seen as high numerically measured wear in Boing et al[8] and in Figure 30, Figure 33 and Figure 34. For S31 and S32 numerically measured wear was lower (in the phenomenological tests) but the tendency to failure is an important additional result. It is therefore suggested that the failures are not secondary to excessive crater but caused by other failure mechanisms. Wear images for lower cutting speed is seen in Figure 42.

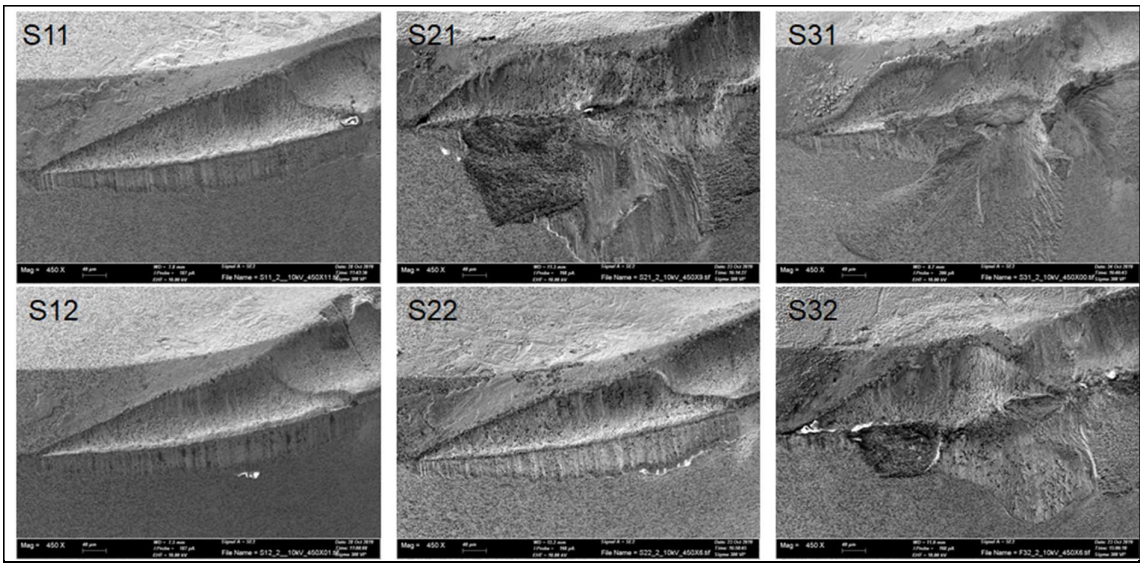

Figure 41: showing wear at the variants run at 270 m/min cutting speed. Retained austenite increase from left to right and hardness incrase from below and up, except for S31/S32 variants both having the same hardness level.

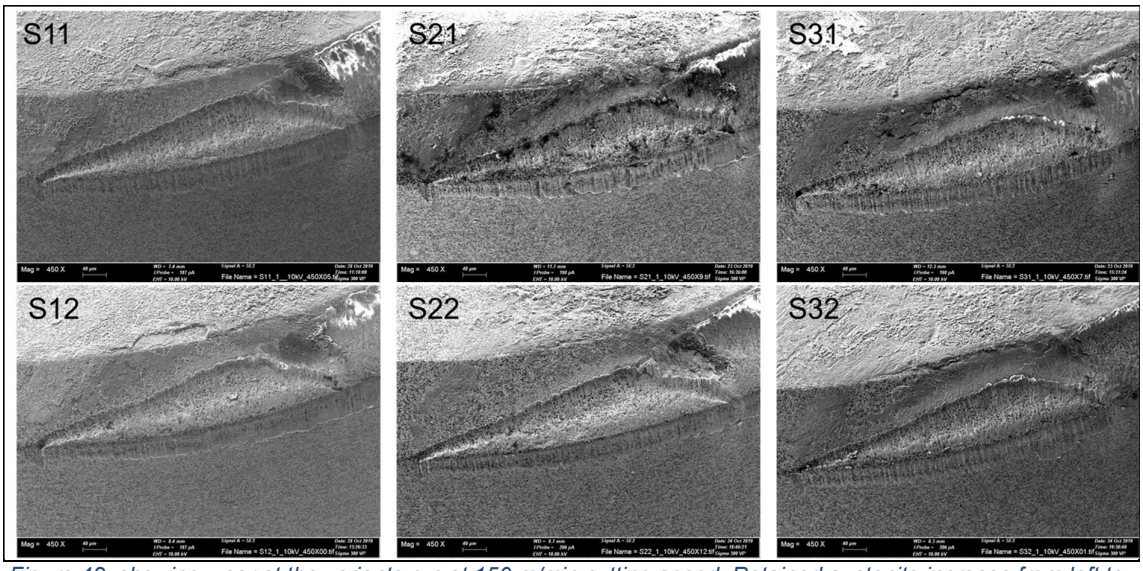

Figure 42: showing wear at the variants run at 150 m/min cutting speed. Retained austenite increase from left to right and hardness incrase from below and up, except for S31/S32 variants both having the same hardness level.

The trend observed in all test set-ups for testing in S-steel (Figure 30), showing an increased tool wear in the 0,72 series is shown here for the differently tempered variants, machined at low and high cutting speed. (Figure 43). In the 0,80 series ~35% retained austenite was formed for which tool wear decrease, creating an anti-optimum around ~25% retained austenite. At high cutting speed the temperature in combination with high amount of

retained austenite create a fatal combination causing tool failure in all tests where zone 1 was included, as discussed to SEM-images above (Figure 43).

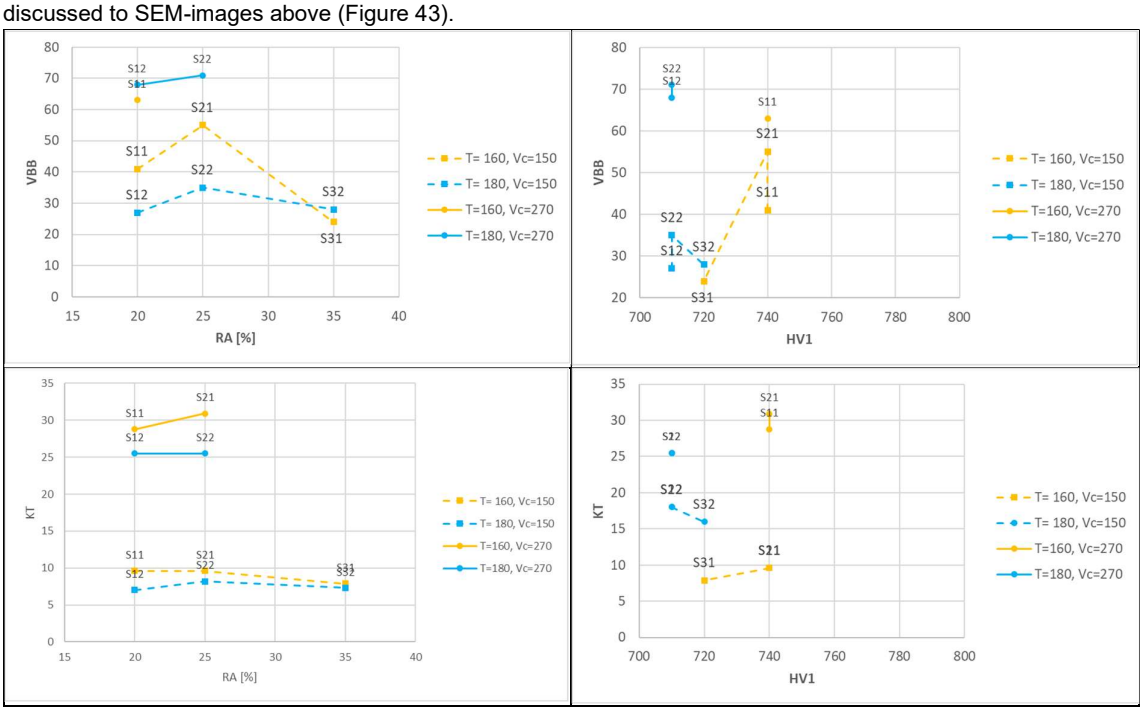

Figure 43: for S-steel showing flank wear (top row) and crater wear (bottom) as function of retained austenite (left panels) and hardness (right panels)

6.4 Impact from machining on retained austenite transformation

The formation of retained austenite formed during heat treatment was also subject of interest in the machining process, as both high load and temperature is induced on the component surface. The same lab components that were analyzed regarding RA by etching was subsequently machined with a worn tool for the study (top images in Figure 44 and Figure 45). Following cutting parameters were used: cutting speed, Vc=210 m/min, feed=0,15 mm/rev and cutting depth 0,1 mm. Retained austenite on the lab components were determined in two ways:

1) On etched surface before and after machining (profiles).
2) On machined surface, at different level from the outer surface (solid markers)

The retained austenite content was compared before and after machining, both on etched surfaces and on machined surfaces, Figure 44. S21 (blue lines) show big deviation between the RA-values before and after machining, especially on 0.2, 0.4 and 0.6mm. Indicates that something has happened during machining. S11 and S31 are more consistent with the measurements before and after machining

The retained austenite was analyzed more closely on the S21 sample, revealing two occurring events close to the surface, Figure 45

- Increase of RA in the outerportion (<10 µm depth), related to white layer formation.
- Decrease of RA in the zone below down to about 0,8 mm, related to a reverse martensite transformation.

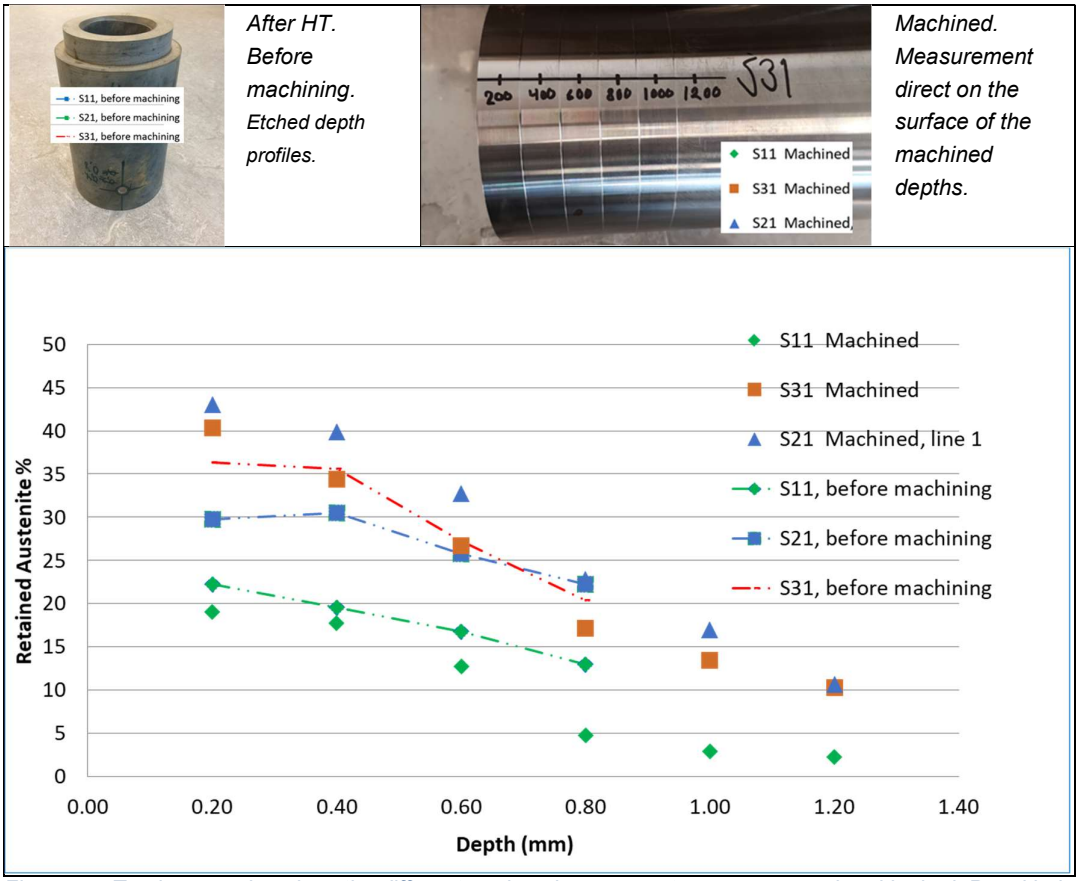

Figure 44: Top images show how the different analyzed components were prepared and looked. Panel below show retained austenite on etched depth profiles before machining (dashed lines) vs surface measurements on machined depth levels (solid markers).

After HT. Before machining. Etched depth profile (S21).

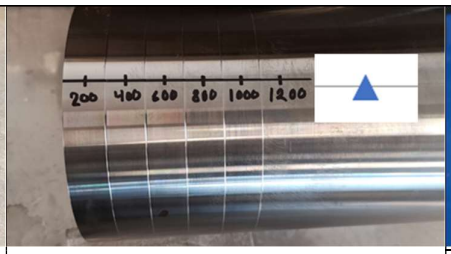

Measurement direct on the surface of the machined depths on S21.

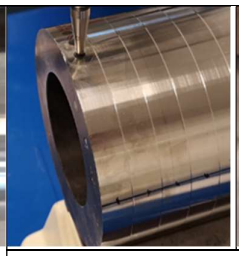

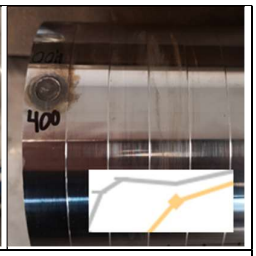

Machined sample. The etched depth profile is located on the machined 200µm surface. Etched depths are 0,15,45,100,200,300 and 400µm

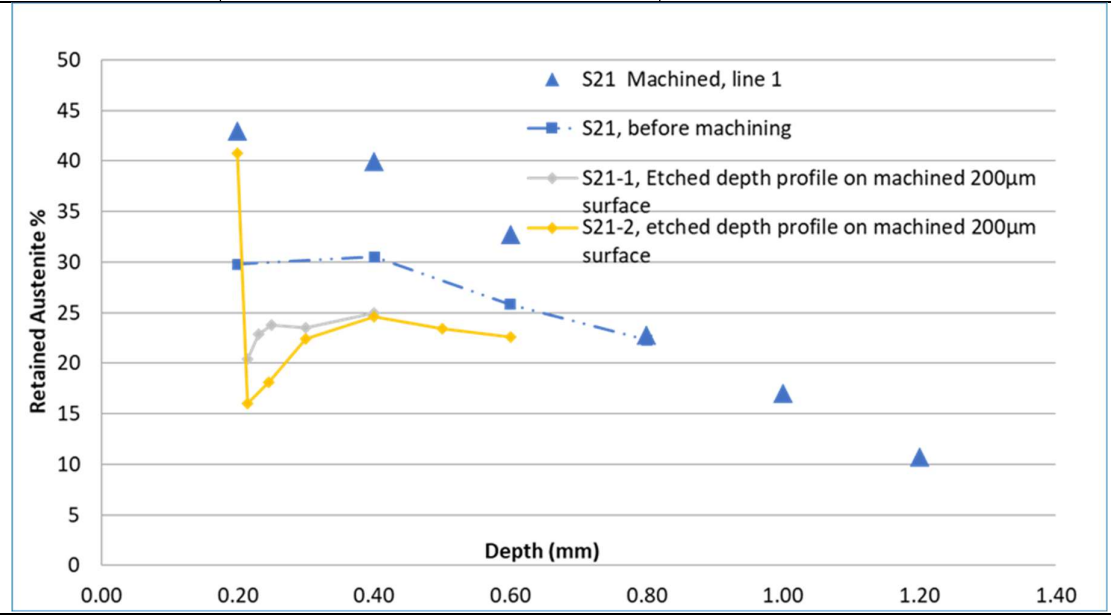

Figure 45: Etched profiles before (dashed) and after machining (filled lines) of lab component S21, surface measurements on machined depth levels is shown by blue triangles.

It was shown in several publications that phase shift can be both thermal and plastically induced [Bedekare et. al. [9], Umbrello et.al.[10]]. Thermo-mechanical induced retained austenite is formed by reverse martensite transformation during machining at temperatures ranging around 550 -650 °C depending on e.g. hardness [Ramesh[11]].

Chou et al[12] show that white layer is formed by tool flank contact (i.e. tool wear) down to 10 µm depth, which is within the analysis range of retained austenite in this study. It was also shown that material heat treatment and cutting speed had a strong correlation to surface alteration, where white layer depth increased with increased cutting speed to a maximum and then asymptotically approach the same value. [Chou et al[12]].

Generally, if there is a thermal white layer formation (TWL) there is a thin layer of newly formed untempered martensite with high amounts of retained austenite and beneath a dark etching layer of over-tempered martensite with reduced amounts of retained austenite and, potentially, below this a layer with a lowered amount of retained austenite due to mechanical effects.

If it is a formation of mechanical white layer (MWL) a very thin top layer is formed whith a complex nano sized microstructure [Hosseini, PhD[13]] and below a layer of reduced amounts of retained austenite due to mechanical

loading. It is difficult to identify a MWL using LOM and to study the MWL itself in detail it is necessary to use high resolution electron microscopy.

It is suggested that both white layer formation, creating more retained austenite in the outer portion of the surface and the transformation of RA on a larger depth from the surface occurred in a specific window of concentrations for retained austenite, carbon content and/or other features that separated S21 from the S11 and S31 samples, Figure 46 and Figure 47.

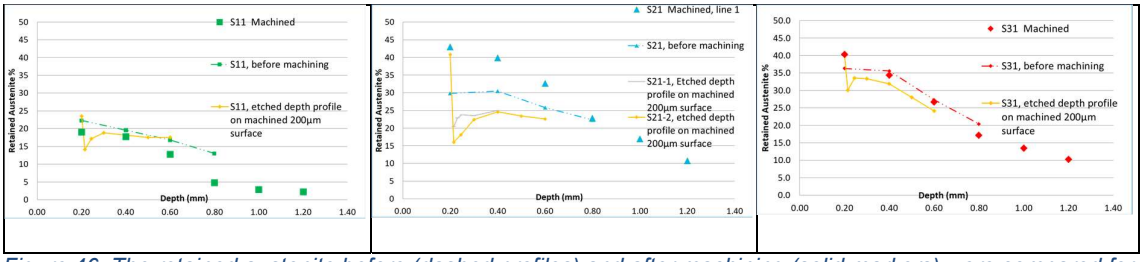

Figure 46: The retained austenite before (dashed profiles) and after machining (solid markers) were compared for carburized variants at 0.64 (left), 0.72 (middle) and 0.80 (right) wt% carbon potential.

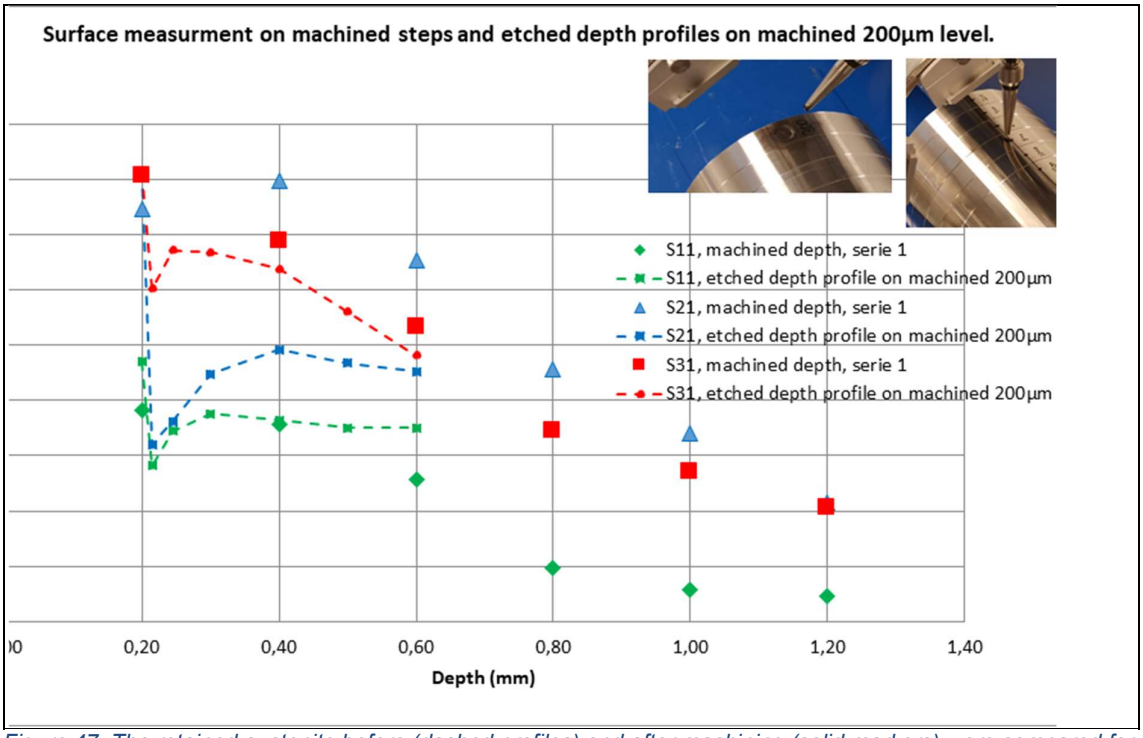

Figure 47: The retained austenite before (dashed profiles) and after machining (solid markers) were compared for carburized variants at 0.64, 0.72 and 0.80 wt% carbon potential.

The results from the characterization show that machining influence the level of retained austenite in the S21 component, but no significant influence for S11 and S31 components Figure 44. It is important to note that the exception, i.e. S21, correlates with the unexpected increase of tool wear, in particular crater wear, in components with retained austenite around 20-25%, i.e. S2X and indicated also for F2X-F3X variants, see Figure 29,Figure 30 and Figure 43.

6.5 Robustness

This study demonstrates the predictive models for estimating the surface roughness of machined components under two cutting speeds from low value to high one. The prediction models are trained and built using multiply regression analysis, support vector regression and multilayer proception modelling approaches with input signal data from time domain and frequency domain in two experimental environments (KTH & Swerim lab). According to the prediction accuracy from different algorithm, the following conclusion are drawn, Figure 48, Figure 49, Figure 50 and Figure 51

1. The support vector regression (SVR) can provide best outcome performances – highest prediction accuracy of surface roughness with input signal data both from time domain and frequency domain. The same conclusion can be drawn if the final results from KTH lab test and Swerim lab test are compared and analyzed.

2. When the prediction is implemented with multiply linear regression modelling approach by the data obtained from KTH lab test, the input data of sound signal from frequency domain enable to increase the prediction accuracy. However, with regard to vibration signal in three directions, the results shows that the vibration signal in time domain outperforms one from frequency domain as input data in term of prediction accuracy. The sound data from Swerim lab test shows there is not any big differences between sound signal in time domain as input data and in frequency as input data.

3. The utilization of vibration and sound signals reconstructed by singular spectrum analysis (SSA) and wavelet packet transform (WPT) can improve the prediction accuracy of multiply linear regression.

4. The vibration and sound signals reconstructed by singular spectrum analysis (SSA) can improve the prediction accuracy of all three learning algorithms.

5. The vibration signals in time domain as inputs of multiply linear regression algorithm provides higher prediction results than when vibration signals in frequency domain as inputs.

6. The captured data from audible sound and vibration in three directions can implement surface quality prediction system building with high prediction accuracy through the support of selected machine learning algorithms.

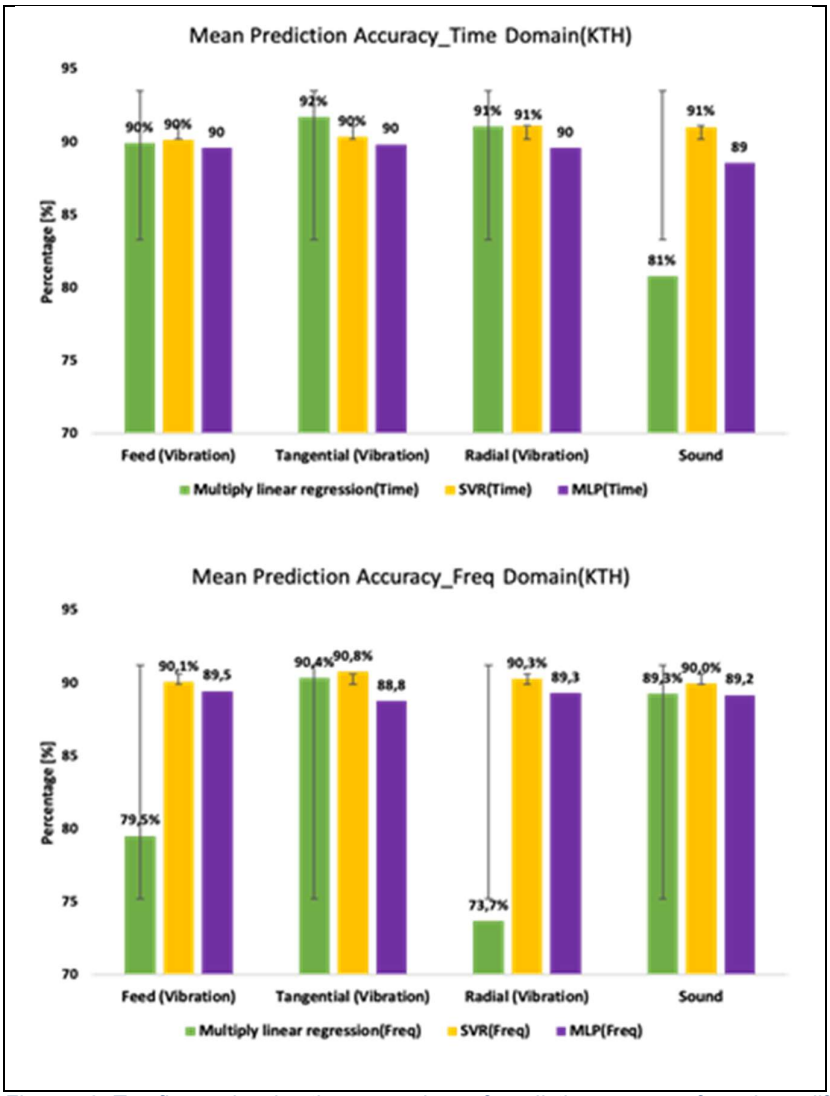

Figure 48: Top figure showing the comparison of prediction accuracy from three different algorithms based on the different signal data in time domain from KTH lab test, bottom figure showing the comparison of prediction accuracy from three different algorithms based on the different signal data in time domain from KTH lab test

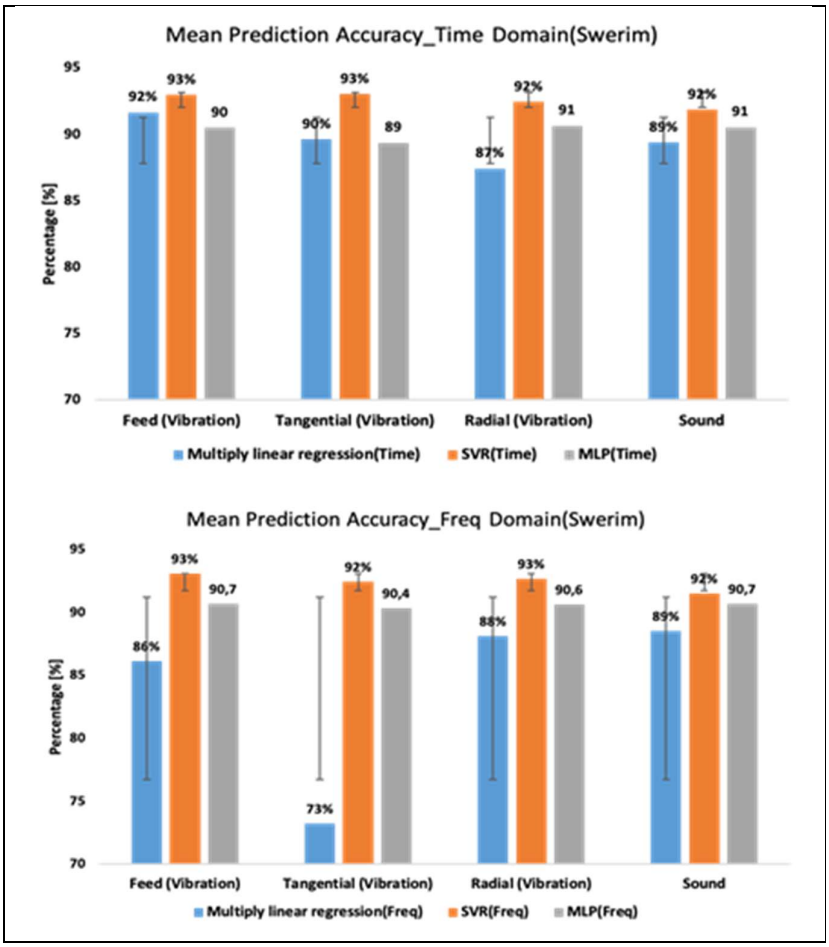

Figure 49: Top figure showing the comparison of prediction accuracy from three different algorithms based on the different signal data in time domain from Swerim lab test, bottom figure showing the comparison of prediction accuracy from three different algorithms based on the different signal data in time domain from Swerim lab test.

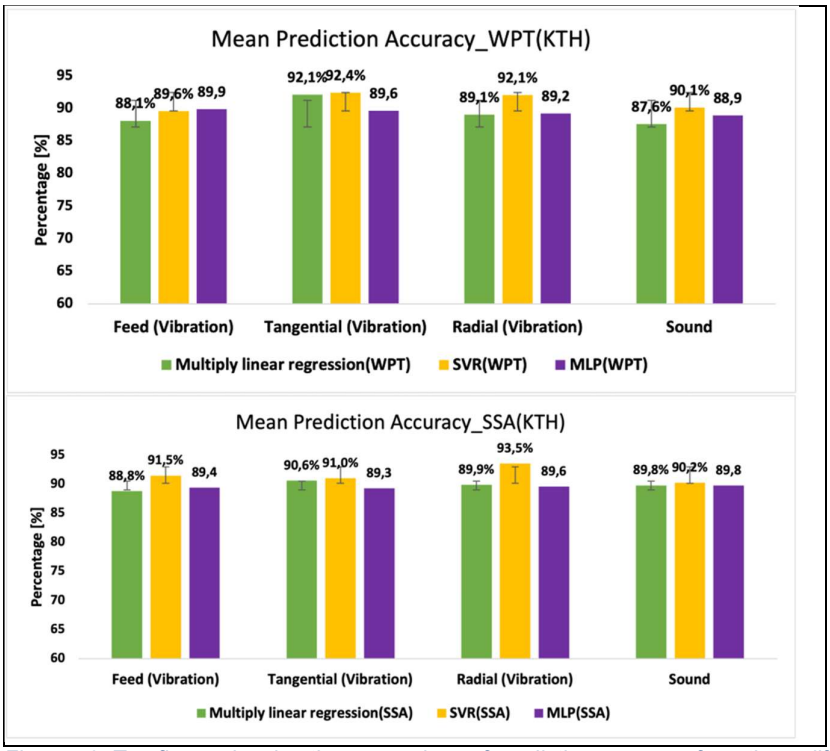

Figure 50: Top figure showing the comparison of prediction accuracy from three different algorithms based on the different signal data reconstructed by WPT from KTH lab test, bottom figure showing the comparison of prediction accuracy from three different algorithms based on the different signal data reconstructed by SSA from KTH lab test.

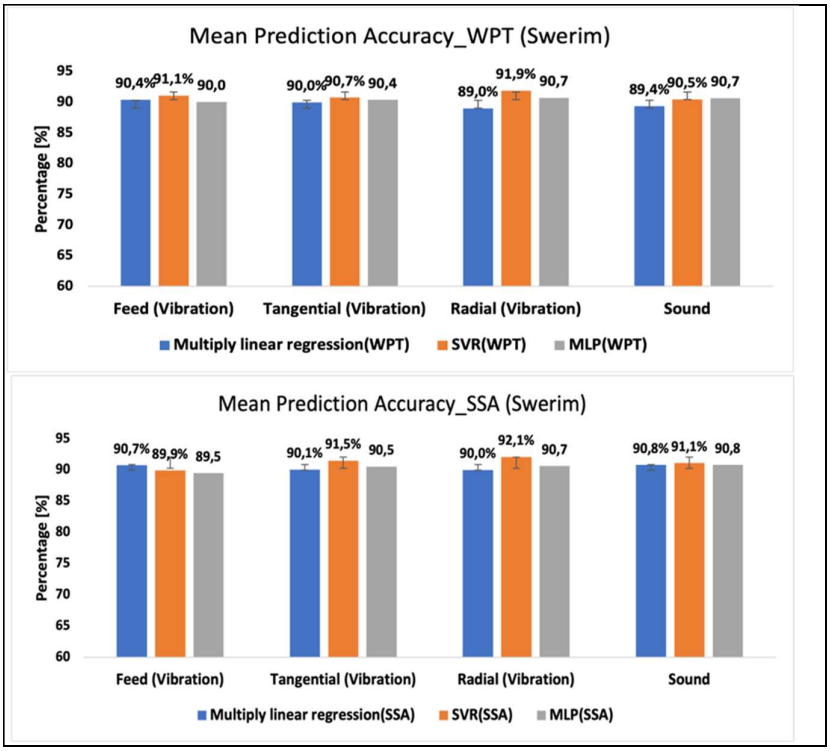

Figure 51: Top figure showing the comparison of prediction accuracy from three different algorithms based on the different signal data reconstructed by WPT from Swerim lab test, bottom figure showing the comparison of prediction accuracy from three different algorithms based on the different signal data reconstructed by SSA from Swerim lab test.

After analyzing and comparing prediction results from different algorithms base on features extracted from signals post-processed with four signal processing approaches, there are some reflections or possible improvements for further deep research work.

- In order to further validate the reliability of research data, more data needs to be collected in each test groups. That is, the number of surface roughness measurement points or data sampling areas on each workpiece should be increased in the new test.
- In this project, all signals and surface roughness are collected and measured with flank wear in very narrow range (between 0 mm – 0.1mm). There should be longer machining time to obtain the complete tool wear progression and corresponding surface roughness development.
- Besides that, the new design of experiments should be totally focused on the purpose and direction of building the surface roughness prediction system – Robustness part. In this project work, the design of experiment cannot completely conform with purpose of research work in robustness area.
- In order to capture full information during the machining, to add other sensors for detecting motor current, cutting force and thermal phenomenon is necessary.
- More efforts and smart methods should be put and studied for achieving automatic selection of many suitable hyperparameters in each algorithm training process.
- The deeper studies of advanced signal processing methods to improve the quality of signals as inputs of each algorithm should be done such as how the different levels of decomposition for each type of signals will impact the signal quality in SSA and WPT and how each different type of mother wavelets applied into WPT influence each signal quality.

7 Demonstrators

Three demonstrators were included in the study for verification of the project results and to give feedback to the production site on their processes. In short they represent studies of varying batches in different in-house furnaces, and comparison of in-house and external furnaces on one batch. Demonstrators are presented separately only the summary is included in this report.

8 Summarizing discussion

A comparison between the steel grades, at given levels of hardness and residual austenite, shows more crater wear for the S type steel than the F. This difference is larger than the impact of hardening variables within a steel, however only at increased cutting speed.
If translated to industrial applications, the selection of steel type may thus be more important than the hardening variables, to design a process with given level of residual austenite and hardness, yet controlled machinability, in particular at increased cutting speed. Expressed differently, selection of an easier-to-machine steel is a means to improve the productivity by increased speed, while keeping given values of residual austenite and hardness.
This should be seen reference to previous work [Björk et.al.[6]], where machinability of different steels in hard part turning were addressed but could not be safely concluded due to variations in hardening outcome. At controlled hardening, the impact of steel grades can now be concluded.

In a subset of data, discussed in a scientific article (Boing et al.[8]), hardness and residual austenite are both seen to drive wear for the S steel – increased wear rate by both higher hardness and higher degree of residual austenite. This subset was seen as the most production-relevant, and had the benefit of pair-wise comparable HV and RA values, However, including the higher-RA variants, the trends do not hold. Instead, a maximum in wear is seen at average RA values, suggesting that different and opposing mechanisms come into play.
Translated to industrial applications, the indication that wear depends on residual austenite, but not in a linear way, would imply that

- In a given process, variations in workpiece material and hardening processes (by intentional variations or scatter) can impact on the machining process by wear and tool life,
- This may give room for optimizations of machining, both by process adjustments and by narrowing of process windows.
- However, it is difficult to establish guidelines, as no simple overall trends are seen.

Multiple edge breakages were also observed for variants with the highest RA values, at higher cutting speed. Controlling the RA levels may therefore be a means of increasing productivity, by more controlled machining – and ability to run at higher cutting speed.

While the demonstrator components from three companies have shown hardness and RA ranges that overlap reasonably well with the experimental lab components, see Figure 52, there are few trends in wear or tool life versus hardening outcome among these.

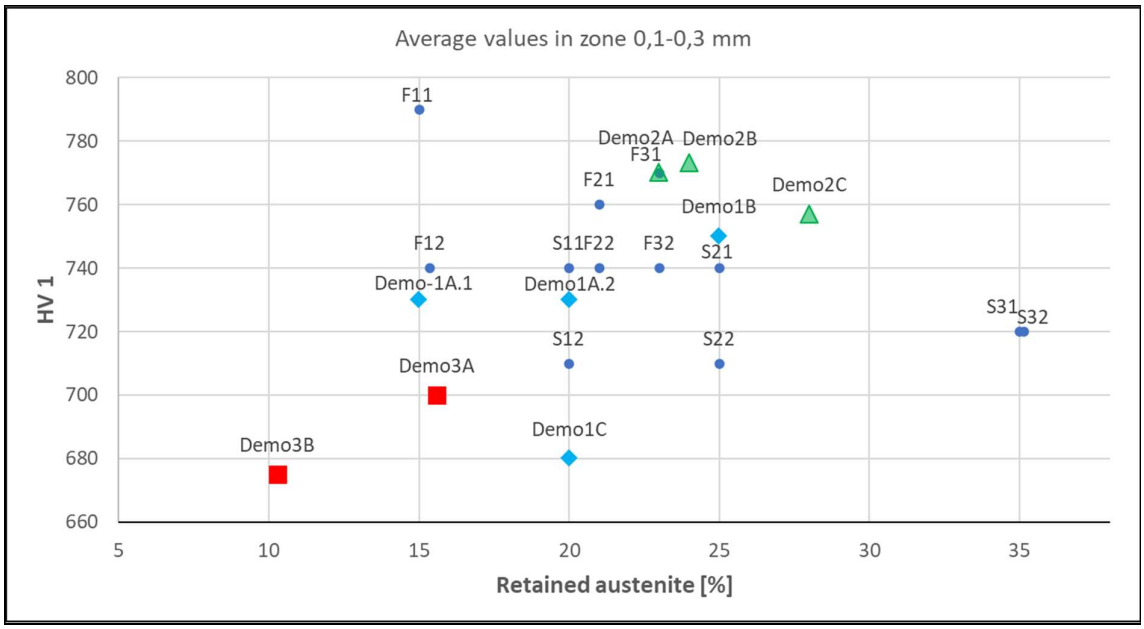

Figure 52: Summary of HV1/RA variants of both lab components (round blue markers) and demonstrator components (blue diamonds-Demo1, green triangles-Demo2 and red squares-Demo3.)

- Demo1: the main difference in material characteristics was between the internal and external flow. For these, initial tool wear results also indicated on differences, but no full wear comparison was possible. For the full-tool-life wear analysis, hardening batches showed very little variation – and correspondingly no significant differences in wear.
- Demo2: despite clear differences in HV and RA for one tested batch, no significant differences were seen in tool wear. It should however be noted that the wear type in this case is mechanical, edge chipping – differing from the more continuous wear modes addressed on the lab components. Moreover, failure is subject to inherent scatter, here combined with some variations of end-of-life criterion for the edges. Therefore, the lack of correlation between wear / degradation and hardening outcome is not in conflict with the results on lab parts.
- Demo3: Clear differences in hardening outcome. Complex outcome on wear and tool life, where internal hardening appears to give more consistent behavior. It is possible that scatter (dimensions) rather than measured RA and HV values explain the outcome in wear and failures.

The industrial importance of controlling hardening processes in terms of material characteristics (RA, HV) is not obvious from the demonstrator examples. Maybe more important is the control of dimensional effects (based on

lab and demonstrator components). It is however believed based on results from lab components that the effects of HV and RA would have an importance also in industrial applications in cases where dimensions are well controlled and the critical wear is crater or flank wear.

The robustness study done in this project was designed to make correlation and prediction of tool wear and surface roughness, which resulted in too little data for the purpose. Therefore, in this project work, the design of experiment cannot completely conform with purpose of research work in robustness area.

9 Conclusion

The material properties (Vickers hardness, HV and retained austenite, RA) in the case hardened portion of lab-components ranged from about 750-800 HV1 and 15-25% RA in 236F, and 700-750 HV1 and 20-35% RA in S159. Flank wear (VB) ranged from about 10 to 80 µm in both steels and crater wear (KT) ranged from 3 to 25 µm KT in 236F and from 8 to 50 µm KT 159S.

Some general trends were defined from the hard part turning tests on lab components:

- The roughing setups show influence of outer scale and distortion
- In steel grade159S there is a possibility to control wear by heat treatment
    - Increased RA and HV drive wear – in selected region
    - Increased RA (%C?) drives risk of edge failure
- Steel grade 236F is less sensitive to variations
    - Less impact from HV and RA
- Tool wear differs between steels grades at similar hardening outcome
    - At higher speed, 236F generates less wear than 159S at similar HV, RA

RA increased during machining in the outer-most portion of the case, to rapidly decrease below the measured RA-profile from case hardening. The effect of phase shift was larger in the same RA-window as identified for increased tool wear.

To verify the methodology for robustness analysis more data is needed. For tool wear prediction, longer sampling of machining data following the wear development is needed.

A mapping of three demonstrators at three production sites showed:

- Variations in hardening outcome between batches and supply routes
- Little impact on machinability
- That possibly other variations dominate (eg distortion/dimensions)

In summary the productivity in industrial applications will benefit from controlled production along the whole production chain!

1.1 References

[1] Holm, Olson, Troell; Steel and it's Heat Treatment – a Handbook, ISBN 978-91-86401-04-7, Swerea IVF (2012)
[2] Hossain et. al, Sci Report 6 (2016) 34958
[3] Hossain et. al, Materials Characterization, 125 (2017) 114-122
[4] Ånmark et.al, "The effect of inclusion composition on tool wear in hard part turning using PCBN cutting tools", Wear 334-335 (2015) 13-22.
[5] Ånmark and Björk, "Tool wear in hard part turning of carburizing steels", KIMAB-2014-502 (2014)
[6] Stavlid and Björk, "Tool wear in hard part turning of carburizing steels 2", KIMAB-2017-119 (2017)
[7] Boing et. al, "Three-dimensional wear parameters and wear mechanisms in turning hardened steels with PCBN tools", Wear 398-399 (2018) 69-78
[8] Boing et. al, "The impact of the retained austenite in case-hardened steels on the crater wear formation of the PcBN tools" Wear *in press* (2021)
[9] Bedekare et. al, "Nanostructural evolution of hard turning layers in response to insert geometry, cutting parameters and material microstructure", CIRP Annals – Manufacturing Technology 62 (2013) 63-66
[10] Umbrello et.al, "Improving surface integrity in orthogonal machining of hardened AISI 52100 steel by modeling white and dark layers formation", CIRP Annals – Manufacturing Technology 58 (2009) 73-76
[11] Ramesh A, "Prediction of Process-induced Microstructural Changes in Orthogonal Hard Machining", Ph.D. Thesis, Mechanical Eng., Georgia Inst. of Technology. (2002)
[12] Chou et. al, "White layers and thermal modeling of hard turned surfaces", Int. J. of Machine Tools & Manufacture 39 (1999) 1863-1881
[13] Hosseini, PhD